To the Graduate Council:

I am submitting herewith a thesis written by Shawn Lee Wesley entitled "An Experimental Study of Solidification of a Pure Melt." I have examined the final copy of this thesis for form and content and recommend that it be accepted in partial fulfillment for the requirements for the degree of Master of Science, with a major in Mechanical Engineering.

Majid Keyhani

Majid Keyhani, Major Professor

We have read this thesis
and recommend its acceptance:

Jay Frankel

Accepted for the Council:

Associate Vice Chancellor and
Dean of The Graduate School

An Experimental Study of Solidification of a Pure Melt

A Thesis
Presented for the
Master of Science Degree
The University of Tennessee, Knoxville

Shawn Lee Wesley
December, 1996

ACKNOWLEDGMENTS

I would like to thank my loving wife for the encouragement that convinced me that I could do anything I put my mind to and to my mother and father for giving me the opportunities I needed to succeed. Last but not least, I would like to thank Dr. Keyhani, Dr. Frankel, and Dr. Parang for their invaluable guidance throughout this project.

ABSTRACT

An experimental study of one-dimensional solidification of n-octadecane was performed. The experimental setup consisted of a cylindrical Plexiglas test cell with a copper heat exchanger positioned at the bottom. Three horizontally mounted thermocouple probes placed at approximately 3, 6, and 9 mm from the cold surface were used to gather temperature data during solidification. The front movement was recorded via a Super-VHS camera from which digital still pictures were obtained for measurement. Several experiments were conducted to simulate conditions for which exact solutions for the solidification are available. The results show excellent agreement with the exact solutions. Two further experiments were completed for conditions that did not have exact solutions in order to extend the benchmark quality data available to researchers of inverse numerical solidification techniques.

TABLE OF CONTENTS

Chapter 1 INTRODUCTION 1
1.1 Importance Of Solidification 1
1.2 Literature Review 2
Chapter 2 EXPERIMENTAL SETUP AND PROCEDURE 5
2.1 Main Setup 5
2.2 Procedure 8
2.3 Uncertainty Analysis 9
Chapter 3 RESULTS AND DISCUSSION 12
3.1 Vertical Probe Data 12
3.2 Horizontal Probe Data 16
Chapter 4 CONCLUSIONS AND RECOMMENDATIONS 35
Bibliography 37
Appendix 39

LIST OF TABLES

Table 1: Measurement uncertainties 9
Table 2: Thermocouple temperature measurement accuracy 11
Table 3: Analysis of Run 1 (vertical probe orientation) 14
Table 4: Analysis of Run 2 (vertical probe orientation) 14
Table 5: Analysis of Run 6 (horizontal probe orientation) 16
Table 6: N-Octadecane properties 16
Table 7: Coefficients of boundary condition curve fit for Run 1 41
Table 8: Front position data for Run 1 42
Table 9 : Coefficients of boundary condition curve fit for Run 2 43
Table 10: Front position data for Run 2 44
Table 11 : Coefficients of boundary condition curve fit for Run 3 45
Table 12: Front position data for Run 3 46
Table 13: Coefficients of boundary condition curve fit for Run 4 47
Table 14: Front position data for Run 4 48
Table 15: Coefficients of boundary condition curve fit for Run 5 49
Table 16 : Front position data for Run 5 50
Table 17: Coefficients of boundary condition curve fit for Run 6 51
Table 18: Front position data for Run 6 52
Table 19: Coefficients of boundary condition curve fit for Run 7 53
Table 20 : Front position data for Run 7 54
Table 21: Coefficients of boundary condition curve fit for Run 8 55
Table 22: Front position data for Run 8 56
Table 23: Coefficients of boundary condition curve fit for Run 9 57
Table 24: Front position data for Run 9 58

LIST OF FIGURES

Figure 1: Experimental setup 6
Figure 2: Horizontal probes 8
Figure 3: Thermocouple calibration data 11
Figure 4: Run 1 with vertical probe orientation, T_i = 29.55 °C 13
Figure 5: Run 2 with vertical probe orientation, T_i = 34.81 °C 13
Figure 6: The effect of axial heat conduction along probe housing 15
Figure 7: Run 3 results, T_i = 29.04 °C 17
Figure 8: Run 4 results 19
Figure 9: Description of the problem with the exact solution 21
Figure 10: Run 5 results, Ste = 5.317 23
Figure 11: Needling solidification 24
Figure 12: Run 6 results, Ste = 5.391 24
Figure 13: Comparison of Runs 5 and 6 26
Figure 14: Non-dimensional temperature data from Run 5, Ste = 5.317, η_{sl} = 0.2976 27
Figure 15: Non-dimensional temperature data from Run 6, Ste = 5.391, η_{sl} = 0.2745 27
Figure 16: Non-dimensional front location for Run 5 28
Figure 17: Non-dimensional front location for Run 6 28
Figure 18: Run 7 results 31
Figure 19:Comparison of Runs 4 and 7 32
Figure 20: Run 8 results, T_i = 40.30 °C 33
Figure 21: Run 9 results, T_i = 29.60 °C 34
Figure 22: Run 1 data 41
Figure 23: Run 2 data 43
Figure 24: Run 3 data 45
Figure 25: Run 4 data 47
Figure 26: Run 5 data 49
Figure 27 : Run 6 data 51
Figure 28 : Run 7 data 53
Figure 29: Run 8 data 55
Figure 30: Run 9 data 57

NOMENCLATURE

C_{ps}	specific heat of solid
C_{pl}	specific heat of liquid
H	heat of fusion
k_l	thermal conductivity of liquid
k_s	thermal conductivity of solid
Ste	Stefan number as defined by Equation 5
t	time
T	temperature
T_c	cold boundary temperature
$T_{c,avg}$	average cold boundary temperature used in exact solution
$T_{c,min}$	minimum temperature of the cold boundary
T_f	melt temperature
T_i	initial temperature
$T_l(\eta)$	temperature at some non-dimensional distance, η, in the liquid
$T_s(\eta)$	temperature at some non-dimensional distance, η, in the solid
V	front velocity
x	linear position from cold surface

Greek

α_l	thermal diffusivity of liquid
α_s	thermal diffusivity of solid
η	similarity variable, non-dimensional distance as described in Equation 6
η_{sl}	similarity variable, non-dimensional position of the solid liquid interface
$\eta_{sl,exact}$	similarity variable, non-dimensional position of the solid-liquid interface obtained from the exact solution described by Equation 2
θ_l	dimensionless liquid domain temperature, defined in Equation 4
θ_s	dimensionless solid domain temperature, defined in Equation 3
ρ_l	density of liquid
ρ_s	density of solid

Chapter 1
Introduction

1.1 Importance of solidification

The ability to predict a solidification process is important in many practical applications such as casting, energy storage, and crystal growth. In casting processes, the rate of solidification and the temperature history of the cast determines the physical properties of the material. Being able to control this process is important in the development of new alloys and in their consistent production. Solidification is also important in designing latent heat thermal energy storage systems. These systems use the latent heat associated with the solidification of substances to store energy, usually energy that would otherwise be lost to the environment or possibly excess energy produced during peak energy generation periods.

Numerical modeling of solidification processes fall into two major categories; direct analysis and inverse analysis. A direct numerical analysis calculates the front motion with respect to time given the boundary conditions of the system, while an inverse numerical technique calculates the boundary conditions required to produce a specified front motion. Direct modeling of solidification processes has been successfully done in the past[1]. However, in recent years, inverse modeling of solidification processes have been more closely studied to provide engineers with the necessary tools to design advanced latent heat energy storage systems and to consistently produce new alloys. Frankel and Keyhani recently developed a numerical method based on a weighted

residual methodology[2]. Their study showed the capabilities of this particular numerical technique to calculate the temperature history required to produce a specified motion. To test the numerical technique, a direct exact solution for the one-dimensional, constant velocity case was used. To further validate this and other inverse numerical techniques, researchers need experimental solidification data where the front movement with respect to time is measured with a high degree of resolution for a variety of boundary temperature histories.

1.2 Literature review

Past experimental studies were conducted either to develop empirical corelations for solidification or to validate an existing numerical prediction technique.

Bathelt et al. [3] conducted a two-dimensional phase-change experiment using solid n-octadecene in a rectangular enclosure with three horizontal heated cylinders placed in the test cell. The purpose was to investigate the effects of natural convection on the heat transfer and melting rates while maintaining a constant heat flux at the cylinders' surface. The shadowgraph technique was used to measure the front movement. They reported local Nusselt number variations at the cylinders' surface and variations of the average heat transfer coefficients through time.

Bathelt and Viskanta [4] conducted another experiment using solid n-heptadecene and solid n-octadecane in a rectangular enclosure with a single horizontal heated cylinder in the test cell. The purpose of this experiment was to develop dimensionless correlations for averaged and local heat transfer coefficients in quasi-steady melting. Their findings

showed that because of the natural convection effects the melting was non-symmetric.

Benard et al. [5] conducted a two-dimensional phase change experiment using solid n-octadecane in a rectangular enclosure with the vertical walls heated at a constant temperature and the horizontal walls being insulated. The purpose of the experiment was to measure the front movement using the temperature measurements from a 5X5 array of thermocouples and visual observations by photographing the front. To measure the front location using the thermocouple array, the solid-liquid interface was assumed to be at the probe location when the thermocouple temperature became greater than the melt temperature of the wax. The results showed good agreement between the two techniques.

Ketkar et al. [1] performed a solidification experiment using caprillic acid in a rectangular enclosure with one vertical wall being cooled. The results from the study were used to validate a numerical solution that utilized the SIMPLER algorithm of Patankar[6] to solve an enthalpy formulation of a two-dimensional phase change problem with natural convection. The experimental results showed good agreement with the numerical procedure.

A study of a two-dimensional phase-change process in a rectangular enclosure with conducting walls was conducted by Ho and Viskanta[7]. They developed correlations for solidification and heat transfer rates for different enclosure aspect ratios. Visual observations were used for front measurements and the shadow graph technique was used to measure local heat transfer coefficients at the heat exchanger surface.

Chun et al. [8] conducted a two-dimensional phase-change study in a cylindrical enclosure to compare with two theoretical prediction techniques. The test cell consisted

of two concentric cylinders with solidification taking place on the inner cylinder. The solid layer's thickness was measured by removing the cold inner cylinder completely from the test cell. Therefore several experimental runs of different durations were needed to document the phenomenon over a range of time for any one set of initial conditions. Their results showed that given the boundary temperature of the inner cylinder, a reasonable approximation of the front movement can be obtained using a formula based on a quasi-steady state assumption.

McDonough and Faghri [9] conducted a phase-change experiment using water inside a rectangular enclosure. The purpose of the experiment was to explore the limitations of a non-intrusive ultrasonic pulse-echo technique in measuring the front position in conduction controlled and natural convection controlled solidification.

The purpose of this study is to produce a high quality experimental database for one-dimensional solidification of a pure melt. N-ocatadecane was chosen as the candidate pure melt, since its thermophysical properties are well documented[10,11]. The results would extend the benchmark quality data available beyond the limited conditions of exact solutions. The data may also be used to verify the accuracy of the numerical models developed for inverse analysis, i.e., given freezing front history, predict the cooling history of the solidification process.

Chapter 2
Experimental Setup and Procedure

2.1 Main Setup

The experimental setup, shown in Figure 1, consisted of a Plexiglas cylinder with a copper heat exchanger positioned at its bottom. The test cell's inner dimensions were 15.875 cm in diameter and 4.25 centimeters tall. A small ruler was positioned inside the cell which enabled the front location to be measured visually. The ruler was made of plastic and was 6 mm wide and 2 mm thick. The test cell was connected to a reservoir to allow additional wax to enter the cell during solidification. Coolant water entered the heat exchanger from the bottom of the setup at the outer edge and passed through a spiral channel exiting at the center. The heat exchanger was instrumented with seven thermocouples mounted in holes drilled into the heat exchanger. These holes allow the thermocouple beads to be placed to within 0.79 mm from the surface of the heat exchanger. All thermocouples were connected to a Hewlett Packard Data Acquisition System which was controlled by a computer.

The first experimental setup (not shown) used five open-end thermocouple probes that were mounted vertically from the top of the test cell. The probe tips were approximately 3, 6, 9, 20, and 40 mm from the heat exchanger surface. The probe housings were made of Inconel with a diameter of 1.59 mm with a type T thermocouple bead secured at the tip with epoxy. The temperature and front data from two initial runs indicated that axial conduction through the probe housing affected the temperature

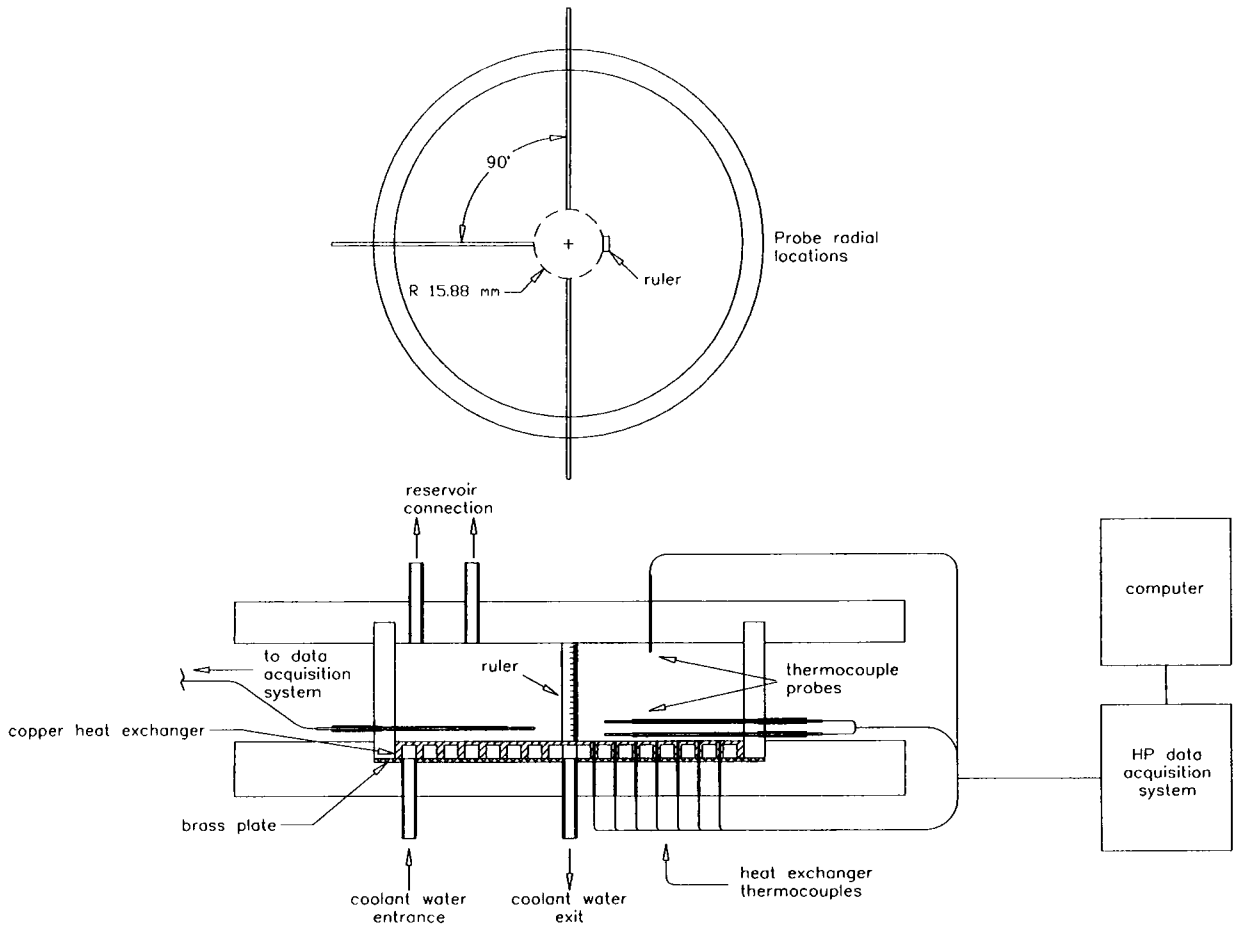


Figure 1: Experimental Setup

measurements. A detailed discussion of the data from these preliminary runs will be given in the next chapter.

To alleviate the problem a new test cell was constructed using three horizontally mounted closed-end stainless steel thermocouple probes with a diameter of 0.51 mm (Figure 1). Orienting the probes parallel to the isotherms of the system ensured that heat transfer through the probe housings would be held to a minimum. The closed-end probes were inserted into ceramic sleeves to increase their stiffness and then inserted into the test cell through holes drilled into the side of the Plexiglas cylinder. The probe tips were placed 15.88 mm from the centerline of the test cell at approximately 3, 6, and 9 mm above the heat exchanger surface. The small diameter of the probes and the fact that they would be supported only from the wall of the test cell, brought into question the stability of the probe tips. This problem was lessened by decreasing the unsupported length of the probes by adding a ceramic and stainless steel sleeve as shown in Figure 2. During the solidification process, the probe locations were not affected by the movement of the front past them. A fourth open ended probe was placed vertically at the top of the test cell. Control of the heat exchanger temperature was achieved through use of two constant temperature baths and a network of valves that allowed the source of the coolant fluid to be quickly changed from one bath to the other. This setup allowed for excellent control over the heat exchanger temperature and provided the means to produce convoluted temperature histories for the heat exchanger.

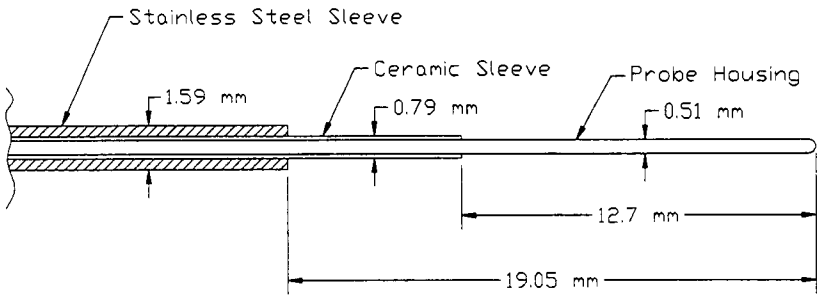


Figure 2: Horizontal probes

To test the uniformity of solidification in the test cell, a test run was made with another ruler placed at the inner wall of the test cell. During the solidification process, no discrepancies between the front location measurements of the two separate rulers could be found.

2.2 Procedure

An experimental run consisted of three stages; the pre-run setup, the run itself where solidification took place and was recorded; and, the post-run data processing.

The purpose of the pre-run setup was to prepare the wax and create the initial condition required for the run (the initial superheat and the desired initial temperature of the heat exchanger fluid). Before each run, the wax was allowed to solidify while under a vacuum to de-air it. Once completely solidified, the wax was re-melted and carefully drained into the test cell. The entire experimental setup was in an enclosure whose temperature could be regulated. Through controlling the enclosure temperature, the initial temperature of the wax in the test cell was maintained to within ± 0.1 °C of the desired value. Several hours were required for the wax to reach a uniform initial

temperature.

To make a run, the computer program which controlled the reading of the thermocouples , the video camera that recorded the front movement, and the constant temperature bath which controlled the heat exchanger temperature were all triggered simultaneously. At the start of a run a visual cue was made on the tape, the coolant water valves were opened, and the computer started collecting temperature data.

After a run was made, the temperature data was converted into a form that could be read by a graphing software program. To process the front movement data, still images from the video tape were digitized and saved on a computer. For each picture the time was recorded and the front position was measured digitally.

2.3 Uncertainty Analysis

The variance present in this study was due to the measurement techniques used to measure the probe locations, the temperatures in the test cell, and the front location. The uncertainties are summarized in Table 1 and a further discussion follows.

Table 1: Measurement Uncertainties

Measured Quantity	Uncertainty
Probe Locations	$\pm$ 0.2 mm
Front Location	$\pm$ 0.11 mm
Temperature	$\pm$ 0.09 °C for 23.0 °C $\leq$ T $\leq$ 34.8 °C
	$\pm$ 0.12 °C for 0.4 °C $\leq$ T $\leq$ 19.6 °C

The probe location were measured using a small metallic ruler with 1/64 of an inch divisions. The measurements taken were estimated to be accurate to at least plus or

minus one half division, which when converted to millimeters, is ±0.2 mm.

The front location was measured using a Super-VHS video camera fitted with an additional lens. The camera was focused on the ruler placed in the test cell during the experiment. After the experiment was complete, still images from the video tape were digitized and saved onto a computer. Using a graphics viewer which would display the pixel coordinates of the cursor when placed on the picture, the front location was measured in pixels. The resolution of the pictures was such that each 1/50 of an inch division on the ruler was 9 pixels in height. The measurement of the front position on the computer was estimated to be within at least ± 2 pixels, which when converted to millimeters becomes ± 0.11 mm.

The temperature measurements were made with closed-end type T thermocouple probes. The probes were connected to a Hewlett Packard Data Acquisition System which measured the voltages produced by the thermocouples. A Basic program running on a connected computer controlled the timing of the measurements and the conversion of the voltages to temperatures. A type T thermocouple placed into a K140/4 Kaye Ice-Point was used to obtain a zero reference temperature. Using the same setup, the probe measurements were compared with two National Bureau of Standards calibrated thermometers. Both the probes and the thermometers were placed in proximity into a constant temperature bath and the temperature readings were compared. Figure 3 shows the results of these measurements and Table 2 summarizes the results. The difference of temperature accuracy between the two temperature ranges was affected by the difference in the temperature resolution of the two thermometers. The thermometer used for 0.3 °C

≤ T ≤ 19.6 °C had a resolution of ± 0.1 °C while the thermometer used for 23.0 °C ≤ T ≤ 34.8 °C had a resolution of ± 0.02 °C. The calibration data shown in Figure 3 shows that for T ≤ 19.6 °C and T ≥ 23.0 °C the respective thermometers had a bias. Therefore the temperature measurement accuracy reported in Table 2 are conservative estimates.

Table 2: Thermocouple temperature measurement accuracy

Temperature Range (°C)	Temperature Accuracy (°C)	Thermometer Resolution (°C)
0.3 °C ≤ T ≤ 19.6 °C	±0.12 °C	±0.1 °C
23.0 °C ≤ T ≤ 34.8 °C	±0.09 °C	±0.02 °C

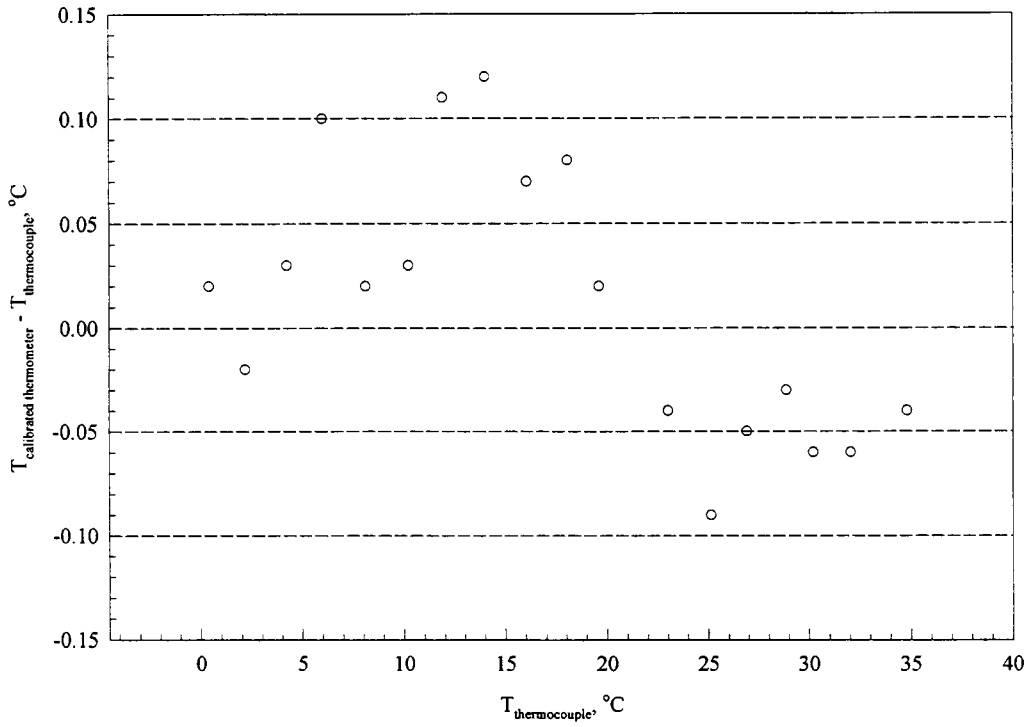


Figure 3: Thermocouple Calibration Data

Chapter 3
Results and Discussion

3.1 Vertical probe data

Two initial runs were made with the vertical probe setup, and the results are shown in Figures 4 and 5. For graphical purposes, the plots of the temperature measured by each of the heat exchanger probes were indistinguishable from each other. Therefore, the cold boundary temperature shown on the plots was obtained by averaging the temperatures measured by each of the thermocouples placed in the heat exchanger at the average time that they were measured.

Examination of the data from both of these runs indicate that the temperature data measured by the probes was inaccurate. This conclusion was reached by comparing the front location data and the temperature data. Under ideal situations, a probe should read 28.15 °C when it comes in contact with the front. For Runs 1 and 2 this is not the case. For example, probe 1 in Run 1 was measured to be 2.88 mm above the heat exchanger surface and fell below 28.15 °C at 399 seconds. However, the front location at 399 seconds was 3.58 mm (a difference of 0.70 mm). This would indicate significant error in either the measurement of the probe's location, the temperature measured by the probe, or the measurement of the front location. Table 3 and 4 summarize the results of repeating the same procedure for all three probes from the two initial runs.

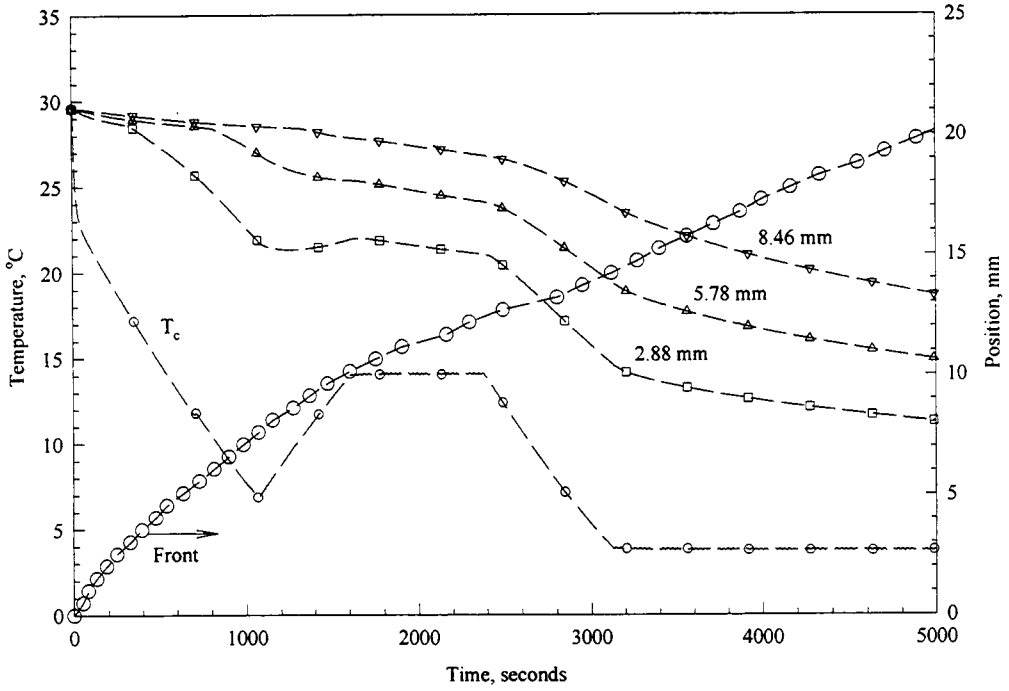


Figure 4: Run 1 with Vertical Probe Orientation, T_i = 29.55 °C

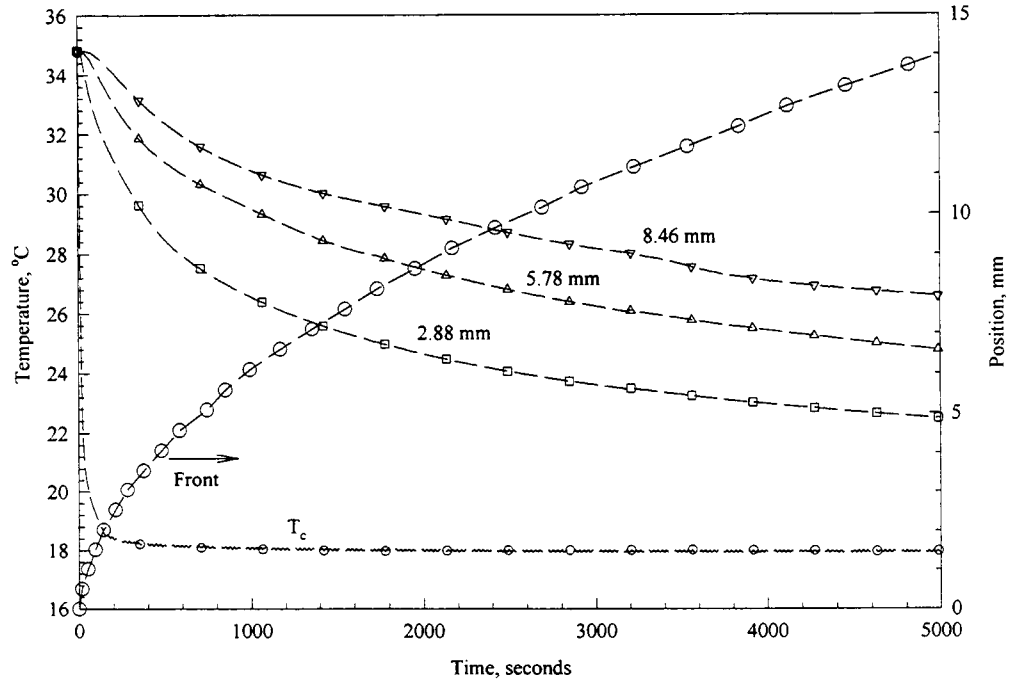


Figure 5: Run 2 with Vertical Probe Orientation, T_i = 34.81 °C

Table 3: Analysis of Run 1 (vertical probe orientation)

Probe Number	Measured probe position, mm	Time Probe fell below 28.15 °C, seconds	Front position at that time, mm	Difference, mm
1	2.88	399.4	3.58	0.70
2	5.78	862.6	6.39	0.61
3	8.46	1431.0	9.44	0.98

Table 4: Analysis of Run 2 (vertical probe orientation)

Probe Number	Measured probe position, mm	Time Probe fell below 28.15 °C, seconds	Front position at that time, mm	Difference, mm
1	2.88	561.7	4.46	1.58
2	5.78	1583.0	7.71	1.93
3	8.46	3038.9	10.86	2.40

Upon reexamination of the probes and the front measurement technique, it was concluded that the temperature measured by the probes was the most likely source of error. Axial heat transfer along the probes caused the wax region at the tip of the probe to remain in the liquid state after the front location had moved beyond the location of the thermocouple as shown in Figure 6. This effect was accentuated during Run 2 where ambient (initial) temperature was 5.5 °C greater than in Run 1. This increased the temperature difference between the top of the probe in contact with the liquid and the bottom of the probe inside the solid. The increase in the temperature gradient increased the axial heat conduction and amplified the effect, which can be seen in Table 4 as an increase in the discrepancy between the front location and measured probe locations.

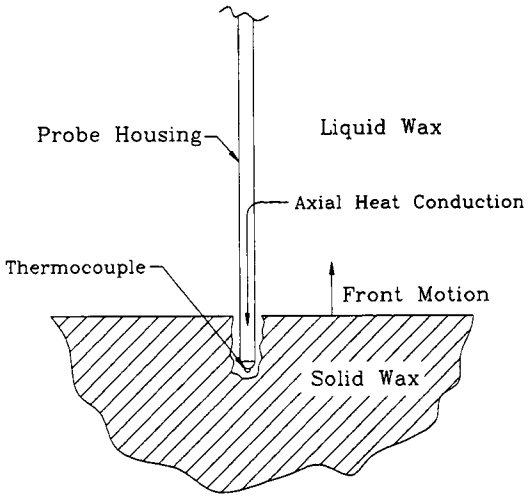


Figure 6: The effect of axial heat conduction along probe housing.

This conclusion was further validated after the setup was rebuilt using horizontally oriented probes and further data was taken. Orienting the probes horizontally, parallel with the isotherms of the system, minimized the temperature variation along the probe housing thus minimizing the axial conduction heat transfer along the probes.

Table 5 shows the analysis of Run 6 with the horizontal probe setup. The temperature and front data show excellent agreement. The front locations fall within the probe measurement range set by the tolerance of the probe location measurement technique.

Run 6 was used for comparison because Runs 3, 4, and 5 were complicated by the fluid becoming supercooled. This will be further discussed in the next section.

Table 5: Analysis of Run 6 (horizontal probe orientation)

Probe Number	Measured probe position, mm	Time Probe fell below 28.15 °C, seconds	Front position at that time, mm	Difference, mm
1	3.37	194.71	3.56	0.19
2	5.95	469.28	6.07	0.12
3	9.23	1001.28	9.27	0.04

3.2 Horizontal probe data

The properties of n-octadecane were taken from Parson et al.[10] and Jin and Wunderlich[11] and are presented in Table 6.

Table 6: N-Octadecane Properties

T_f= 28.15 °C
H = 241730 J/kg
ρ_l = 774 kg/m^3
k_l = 0.15 W/(m·K)
C_{pl} = (2145.9 + 2.8837T) J/(kg·°C)
ρ_s = 814 kg/m^3
k_s = 0.43 W/(m·K)
C_{ps} = (-4624.4 + 243.39T) J/(kg·°C), for 26.85 °C < $T \leq$ 28.15 °C
C_{ps} = (1655.5 + 9.606T) J/(kg·°C), for $T \leq$ 26.85 °C

Figure 7 shows the results from Run 3. The purpose of this run was to provide experimental front and temperature data for comparison with an ongoing inverse numerical study. The probes were measured to be 3.18, 5.95, and 9.13 mm above the surface of the heat exchanger. The probe diameter is 0.51 mm, therefore the temperature measured by each probe will be an "average" temperature over the height range from the bottom to the top of the probe. The heat transfer phenomenon that governs the

temperature measured by each thermocouple probe is not investigated here. Rather, after a run was made and the front location data was processed, the same procedure that was used to discover the discrepancies of the initial runs was used again to calculate the effective "thermal location" of the probes. The temperature data was examined to determine at what time each probe fell below the melt temperature of the wax. Interpolating the measured front location at this time implied the effective location of each probes, which was within ± 0.51 mm (probe diameter) of the measured location of each probe.

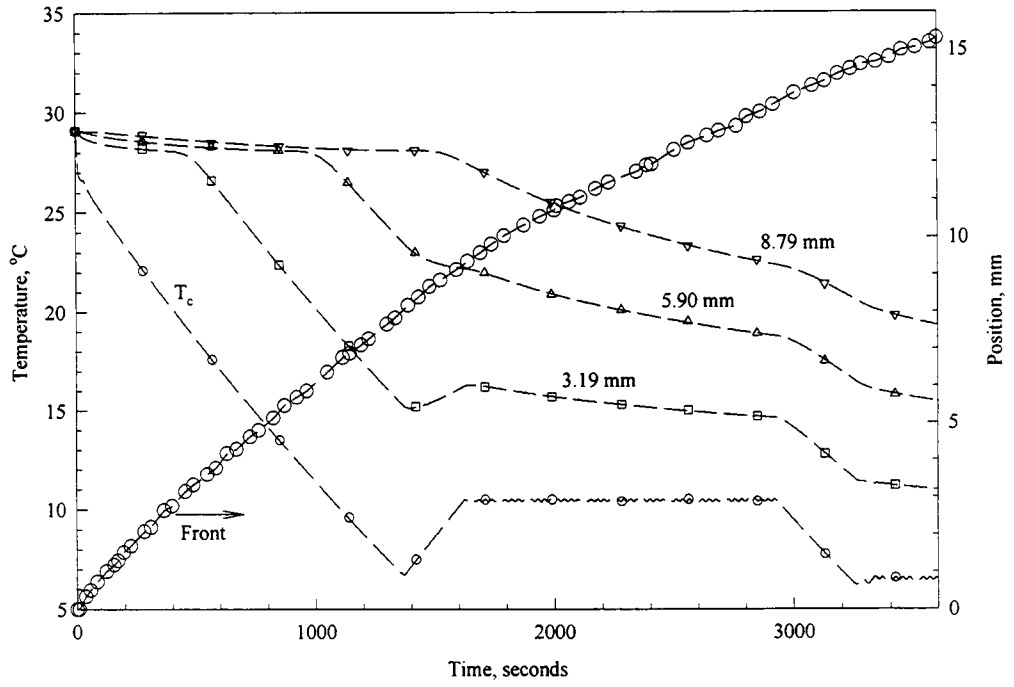


Figure 7: Run 3 Results, $T_i = 29.04$ °C

One complication that arose for runs 3, 4, and 5, where the initial temperature was close to T_f, was that the probe temperatures stabilized slightly lower than 28.15°C before the front could reach them. In these cases, the effective thermal location of the probes

were found by determining when the probe temperature began to steadily drop. Using the latter method for Run 3, the effective thermal locations of the probes was found to be 3.19, 5.90, and 8.79 mm, respectively.

Figure 8 shows the results from Run 4. The purpose of this run was to obtain a constant velocity front movement and compare the results to an exact solution for this case obtained from Carslaw and Jaeger[12]. For a pure melt initially at its fusion temperature, T_f, with constant velocity front motion, V, the temperature history at any location, x, above the cool surface can be calculated by

$$T(x,t) = T_f + \frac{H}{C_{ps}}\left[1 - e^{\left(\frac{V^2}{\alpha_s}t - \frac{V}{\alpha_s}x\right)}\right] \text{ for } x \le Vt \qquad (1)$$

where H is the heat of fusion and C_{ps} is the specific heat of the material. For $V^2t/\alpha < 1$, the exact solution suggests that a nearly linear decrease in the boundary temperature will results in a constant front velocity solidification process. The C_{ps} used in the exact solution was found by calculating the property at an average wax temperature,

$$\frac{\left(T_f + T_{c,\min}\right)}{2} = 15.08^{o}\text{C}$$

where $T_{c,min}$ is the cold boundary temperature at 2000 seconds.

Before this run was made the location of the thermocouple probes were measured to be 3.27, 6.15, and 9.23 mm. These measurements are from the heat exchanger surface to the middle of the probes. The effective probe locations were found to be 3.68, 6.36,

and 9.19 mm which fall within the measured height ranges discussed earlier. The effective probe locations were used to obtain the predictions by the exact solution.

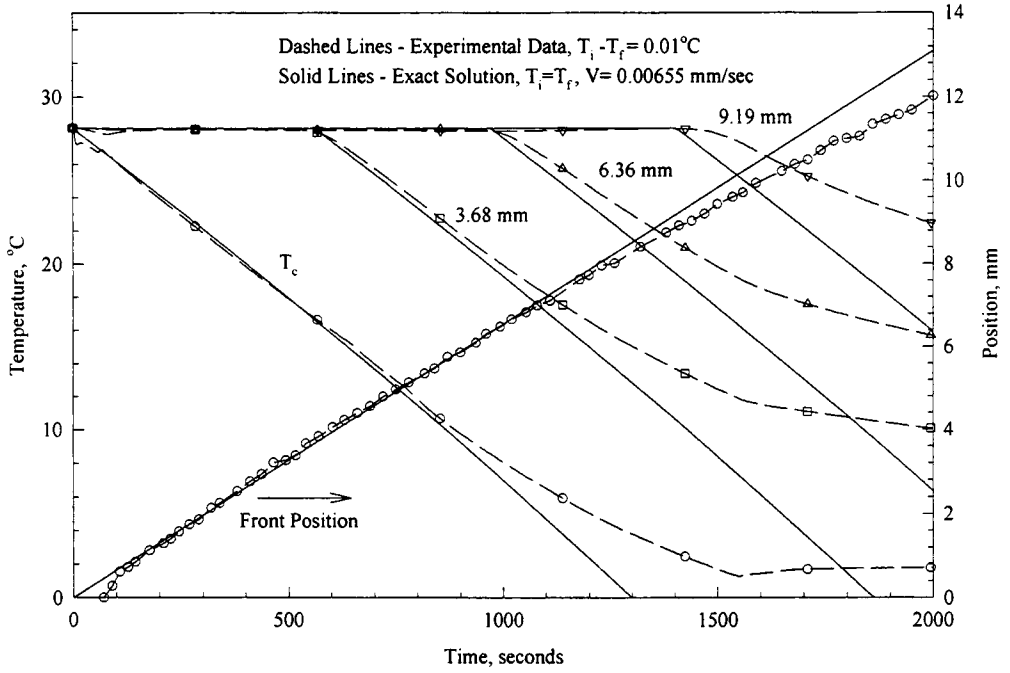


Figure 8: Run 4 Results

The initial pause in solidification, shown in Figure 8, was due to supercooling of the fluid[13]. Supercooling is a term used to describe the physical phenomenon of a liquid being brought below its fusion temperature without solidification occurring. Once solidification began, the front proceeded with a nearly constant front velocity. After 900 seconds the constant temperature bath controlling the heat exchanger could not maintain the nearly linear temperature drop required to produce the constant velocity front, therefore the front velocity decreased. From 127 to 1110 seconds the front velocity was nearly constant at 0.00655 mm/s. During this time, the average difference between the theoretical and the experimental front position was 0.06 mm with the maximum

difference being 0.17 mm at 465 seconds. Also, for $t < 900$ second, the measured probe temperature at $x = 3.68$ mm is in very good agreement with the exact solution.

The purpose of Run 5 was to attempt to simulate a step change boundary condition in a single phase , i.e., $T_i = T_f$, solidification process. An exact solution for this case was used for comparison[14]. If a pure melt at some initial temperature, T_i, equal to or above it fusion temperature, T_f, in a one dimensional system as shown in Figure 9 is subjected to an instantaneous decrease in the bottom boundary temperature from T_i to some T_c less than T_f, then the front motion and temperature history at any distance, x, from the bottom can be determined from the following equations.

Solid-Liquid Interface Location:

$$\frac{T_f - T_i}{T_f - T_c}\frac{k_l}{k_s}\sqrt{\frac{\alpha_s}{\alpha_l}}\frac{\exp\left[-(\alpha_s/\alpha_l)\eta_{sl}^2\right]}{\operatorname{erfc}\left(\sqrt{\alpha_s/\alpha_l}\,\eta_{sl}\right)} + \frac{\exp\left(-\eta_{sl}^2\right)}{\operatorname{erf}\left(\eta_{sl}\right)} - \mathrm{Ste}\sqrt{\pi}\eta_{sl} = 0 \qquad (2)$$

Solid-domain Temperature Solution:

$$\theta_s = \frac{T_s - T_c}{T_f - T_c} = \frac{\operatorname{erf}(\eta)}{\operatorname{erf}\left(\eta_{sl}\right)} \qquad 0 < \eta < \eta_{sl} \qquad (3)$$

Liquid-domain Temperature Solution:

$$\theta_l = \frac{T_l - T_i}{T_f - T_i} = \frac{\operatorname{erf}\left(\sqrt{\alpha_s/\alpha_l}\,\eta\right)}{\operatorname{erf}\left(\sqrt{\alpha_s/\alpha_l}\,\eta_{sl}\right)} \qquad \eta_{sl} < \eta < \infty \qquad (4)$$

where T_s is the temperature at some point, x, in the solid, T_l is the temperature at some point, x, in the liquid, and the Stefan number, *Ste*, and η are defined as

$$\text{Ste} = \frac{H}{C_{ps}\left(T_f - T_c\right)}, \tag{5}$$

and

$$\eta = \frac{x}{2\sqrt{\alpha_s t}}, \tag{6}$$

respectively. For a given set of parameters, the non-dimensional solid-liquid interface location, η_{sl}, can be solved for numerically using Equation (2). Once η_{sl} has been found, Equation (6) can be used to calculate the front location, x, at any time, t, and Equations (3) and (4) can be used to calculate the solid and liquid domain temperatures at any x location, respectively. The non-dimensional solid and liquid domain temperatures, θ_s and θ_l, are defined for use in a later discussion.

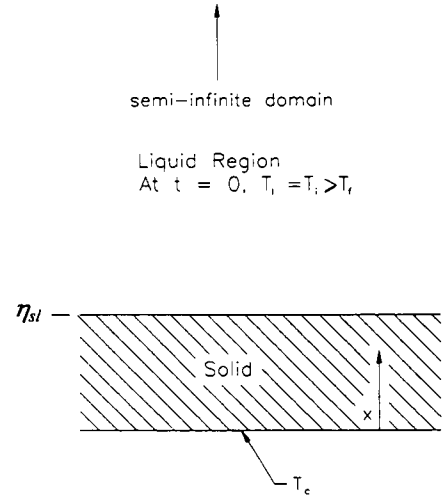


Figure 9: Description of the problem with the exact solution

It should be noted that even though the equations call for separate liquid and solid densities, Poulikakos's formulation of the problem does not account for liquid movement

toward the front due to the change in density during the solidification process. The formulation assumes constant properties. The values for C_{pl} and C_{ps} used in the exact solution were evaluated at $(T_i + T_f)/2$ and $(T_f + T_{c,avg})/2$, respectively.

Figure 10 shows the results from Run 5. The boundary temperature used in the exact solution was $T_{c,avg} = 2.96$ °C and was found by averaging the heat exchanger temperature from 450 to 1000 seconds. The thermocouple probe positions were measured to be 4.56, 6.95, and 9.53 mm. These measurements were taken from the heat exchanger surface to the middle of the probes. Examining the temperature and measured front data implied the effective probe locations to be 4.15 mm, 6.92 mm, and 9.11 mm. The probe temperatures for this run stabilized slightly lower than 28.15 °C so the measured front data and time at which each probe temperature began to steadily drop was used to determine the effective location of each probe.

Both the front position and the 4.15 mm probe's temperature data deviated somewhat from the exact solution during the first 500 seconds because of the inability to simulate the step change boundary condition. Considering the fact that the experimental cooling condition is by no means a step change in the boundary temperature, the agreement between the data and the prediction is surprisingly good. The average difference between the theoretical and experimental front location was 0.24 mm with a maximum difference of 0.70 mm at 9 seconds. After the initial 500 seconds where the deviations from the step change boundary condition occur, the average difference becomes 0.18 mm with the maximum difference being 0.60 mm at 2296 seconds.

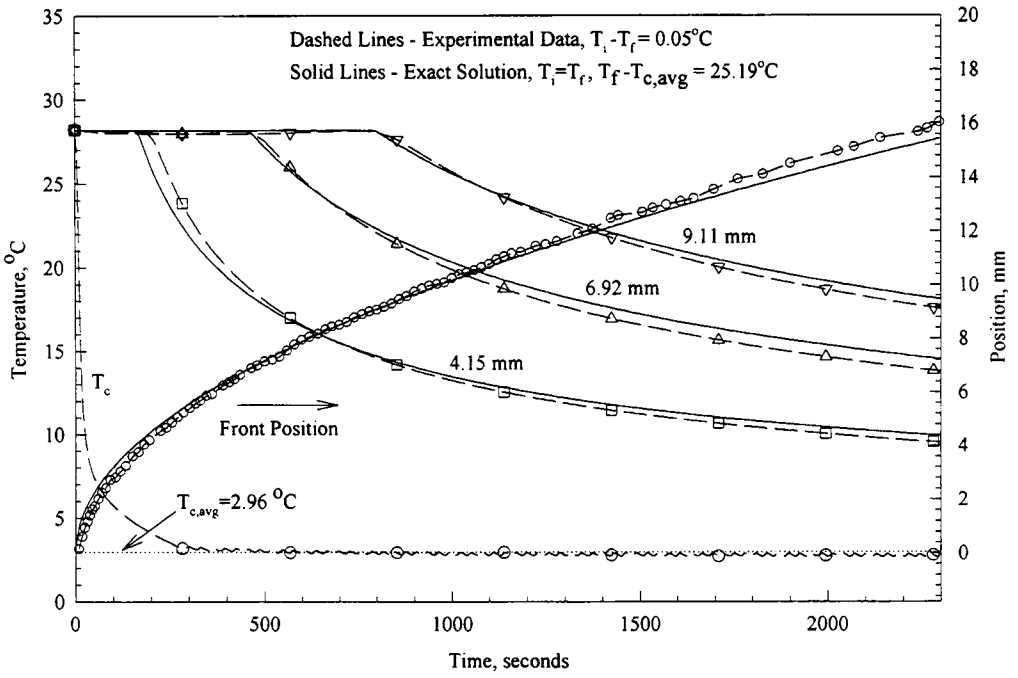


Figure 10: Run 5 Results, Ste = 5.317

After approximately 1200 seconds, the measurement of the front location was hampered by needling solidification of the wax on the sides of the test cell as illustrated in Figure 11. This "needling" on the sides of the test cell appears when the initial conditions are such that axial conduction cooling through the walls of the test cell is sufficient to cause local solidification on the inner surface of the Plexiglas cylinder.

Figure 12 shows the results from run 6. The purpose of this run was to attempt to simulate a step change boundary condition for a superheated melt and compare the results with the exact solution; i.e., predictions obtained from Equations (2), (3), and (4). The boundary temperature used in the exact solution was $T_{c,avg}$ = 3.33 °C and was found by averaging the heat exchanger temperature from 450 to 1000 seconds. The initial superheat of the melt was T_i - T_f = 10.85 °C. The probe locations were measured before

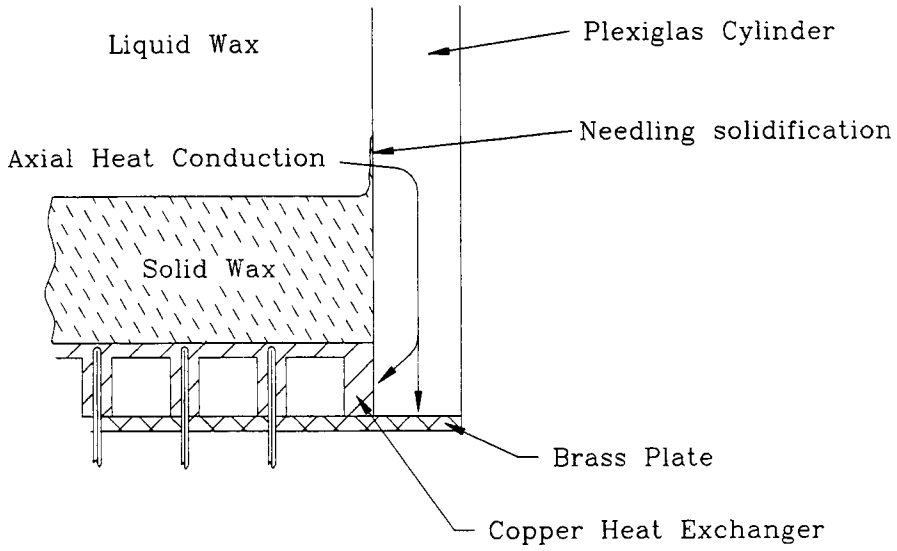


Figure 11: Needling solidification

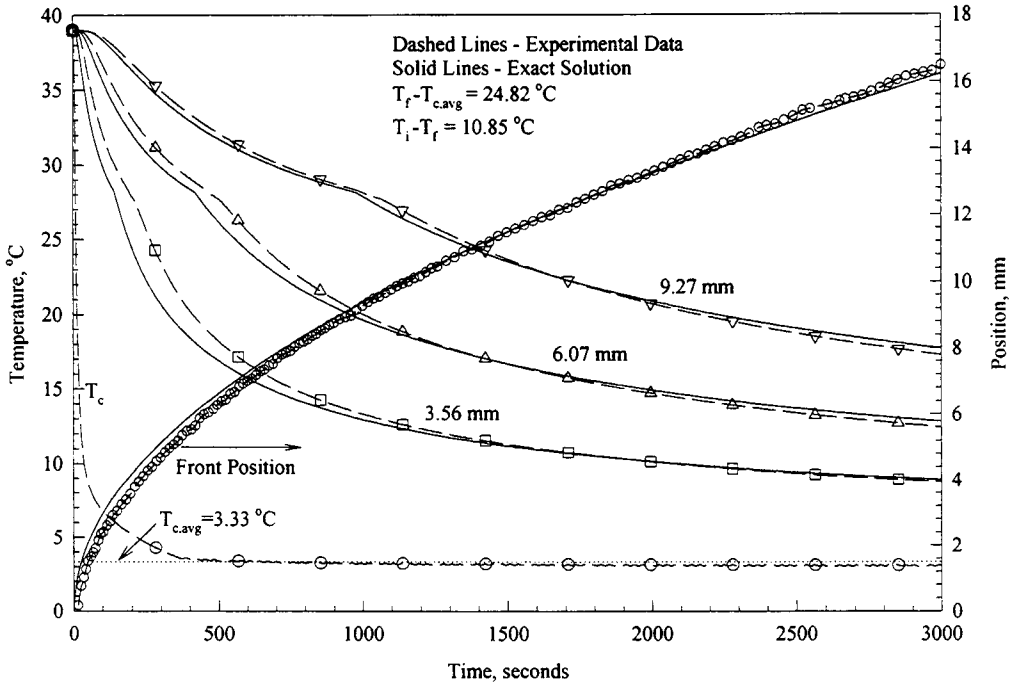


Figure 12: Run 6 Results, Ste = 5.391

the run to be 3.37, 5.95, and 9.23 mm. These measurements were taken from the heat exchanger surface to the bottom of the probes. After the run, the effective location of the probes were found to be 3.56 mm, 6.08 mm, and 9.27 mm.

The results show the same deviations from the exact solution caused by the inability to reproduce a step change boundary condition as in Run 5. However, for Run 6 this effect is amplified by the initial superheat of the melt which causes the probe temperatures to be higher than the exact solution. The average difference between the exact solution and the experimental front data was 0.23 mm with the maximum difference of 0.98 mm occurring at 15 seconds. Excluding the initial 500 seconds, the average difference was 0.13 mm with a maximum of 0.36 mm occurring at 525 seconds. Needling along the sides of the test cell was not a factor because of the initial superheat.

Figure 13 shows a comparison of boundary conditions and front movements of Runs 5 and 6. As would be expected, the front motions are similar in shape but the increase of the initial superheat in Run 6 decreased the rate of solidification for the similar boundary cooling conditions.

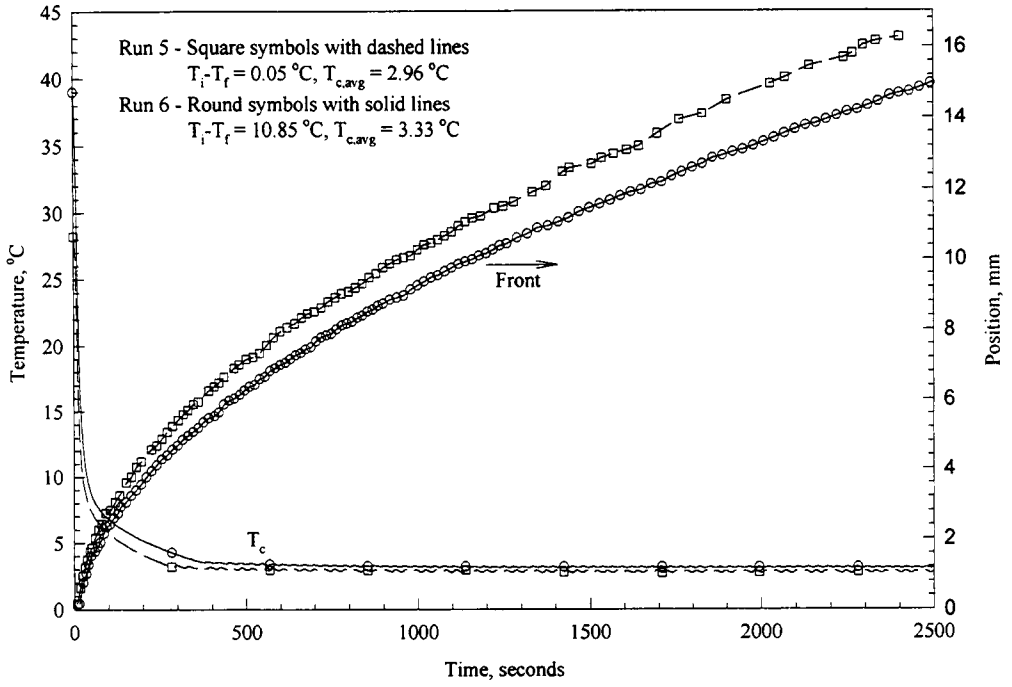


Figure 13: Comparison of Runs 5 and 6

Figures 14 through 17 are non-dimensional representations of the data from Runs 5 and 6. Using the definition of η, η_{sl}, θ_l, and θ_s, the data was cast in non-dimensional form and compared with the non-dimensional exact solution.

Figure 14 is a plot of the temperature data from Run 5 cast into non-dimensional form by using Equation 3. The formulation of the problem splits the temperature solutions into the solid domain (Equation 3) and liquid domain (Equation 4). Therefore, the temperature data taken by each probe must be separated into the measurements taken while in the liquid and measurements taken while in the solid. The fluid temperature solution of in Run 5 is not shown, since its initial conditions were meant to simulate a melt with no initial superheat. For each temperature data point acquired by a probe, the x position of the probe and the time at which the temperature was measured are used to

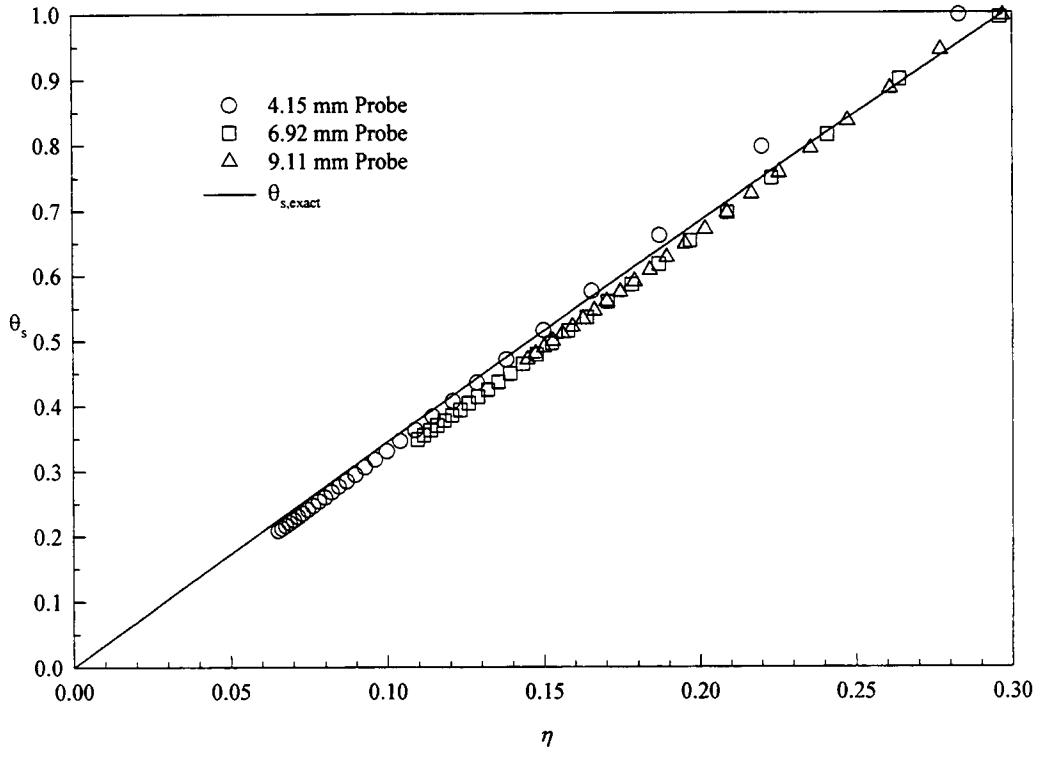


Figure 14: Non-dimensional temperature data from Run 5, Ste = 5.317, $\eta_{sl} = 0.2976$

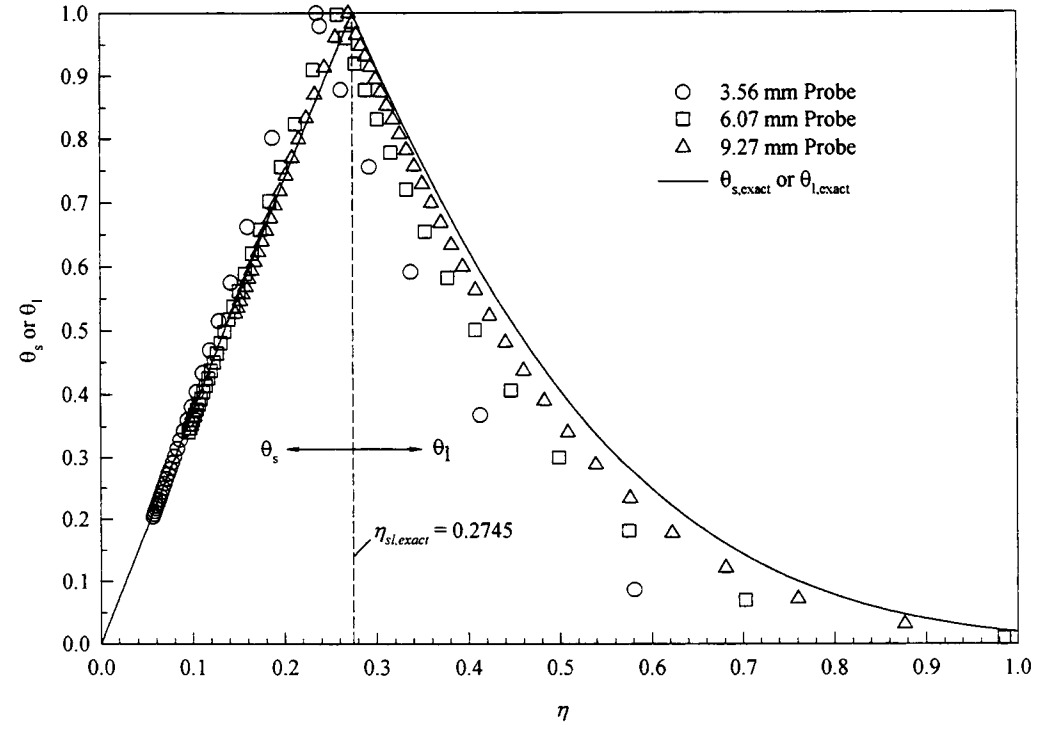


Figure 15: Non-Dimensional Temperature Data from Run 6, Ste = 5.391, $\eta_{sl} = 0.2745$

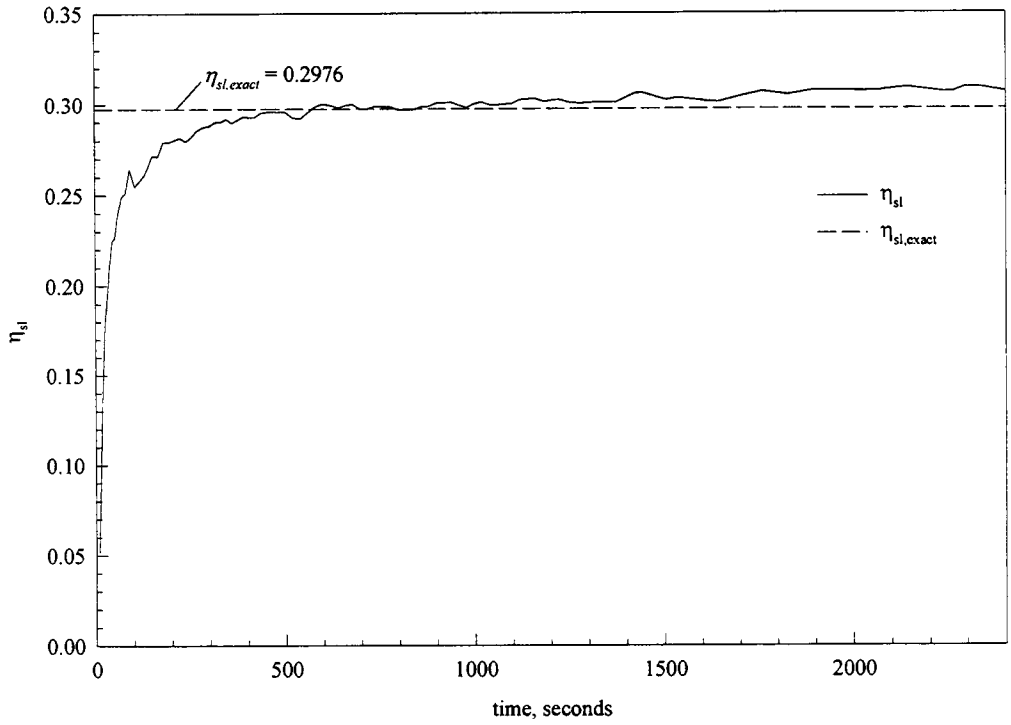


Figure 16: Non-Dimensional Front Location for Run 5

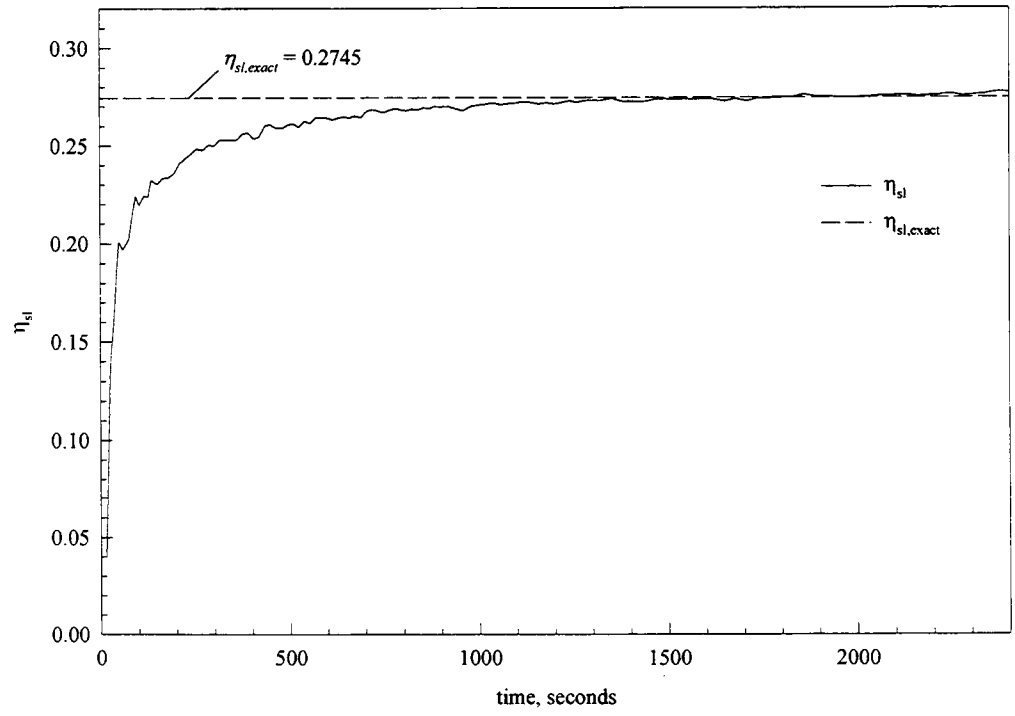


Figure 17: Non-Dimensional Front Location for Run 6

calculate an η, while the temperature measurement is transformed into θ_s using the fusion temperature of the wax and the average cold boundary temperature used in the exact solution. For clarity, only every fortieth data point is shown.

Figure 15 shows the temperature data from Run 6 cast in non-dimensional form. The initial superheat of Run 6 allows for a comparison of the liquid temperature solution also. The plot of the non-dimensional temperatures for the solid and liquid domains can be combined on one plot, realizing that any η greater than $\eta_{sl,exact}$ for Run 6 ($\eta_{sl,exact}$ = 0.2745) is in the liquid region and is defined by Equation 4. Only every fortieth data point is shown for the solid region, with every tenth data point shown for the liquid region.

Both Figure 14 and Figure 15 show good agreement between the non-dimensional form of the experimental data and the exact solution, despite the inability of the experimental setup to produce the step change boundary condition assumed by the exact solution. The results from Run 6 show larger deviations from the exact solution in the solid region, which is most likely due to the initial superheat amplifying the affects of the inability to produce the step change boundary condition.

Figure 16 and 17 show the results of transforming the front data into the non-dimensional form and comparing it with the exact solution front location. For each front data point, the position of the front, x, and the time at which it was measured, t, were used to calculate a non-dimensional η_{sl} using Equation 6. The experimental η_{sl} was then plotted with respect to time and compared with the exact solution front location calculated from Equation 2.

The results from both runs show large deviations from the exact solution during the initial 500 seconds of each run caused by the inability to produce the step change boundary condition. The average experimental η_{sl} from 500 to 1500 seconds for Run 5 was 0.2996 with the exact solution being 0.2976. The average experimental η_{sl} from 500 to 1500 seconds for Run 6 was 0.2688 with the exact solution being 0.2745.

Figure 18 shows the results from Run 7. The purpose of this run was to produce the same linear boundary temperature drop as in Run 4 but increase the initial superheat and measure its effect on the solidification process. Ice was added to the constant temperature bath that controlled the heat exchanger at approximately 950 seconds in an attempt to prolong the linear temperature drop. The probe heights were measured to be 3.37, 5.95, and 9.23 mm. These measurements were taken from the heat exchanger surface to the bottom of the probes. The effective location of the probes were found to be 3.90, 6.22, and 9.49 mm, respectively.

The front movement data shows a time-lag caused by the initial superheat and also shows the pause in the solidification due to supercooling of the fluid at the boundary as in Run 4. Adding the ice to the constant temperature bath enabled the nearly linear temperature drop to be maintained until 1100 seconds. This allowed the front velocity to remain approximately constant from 300 to 1300 seconds, where the average velocity of the front was calculated to be 0.00596 mm/sec. For reference, Figure 18 shows a constant velocity front position with V = 0.00596 mm/sec.. During this time, from t = 300 to 1300 seconds, the average difference between the constant velocity solidification process and

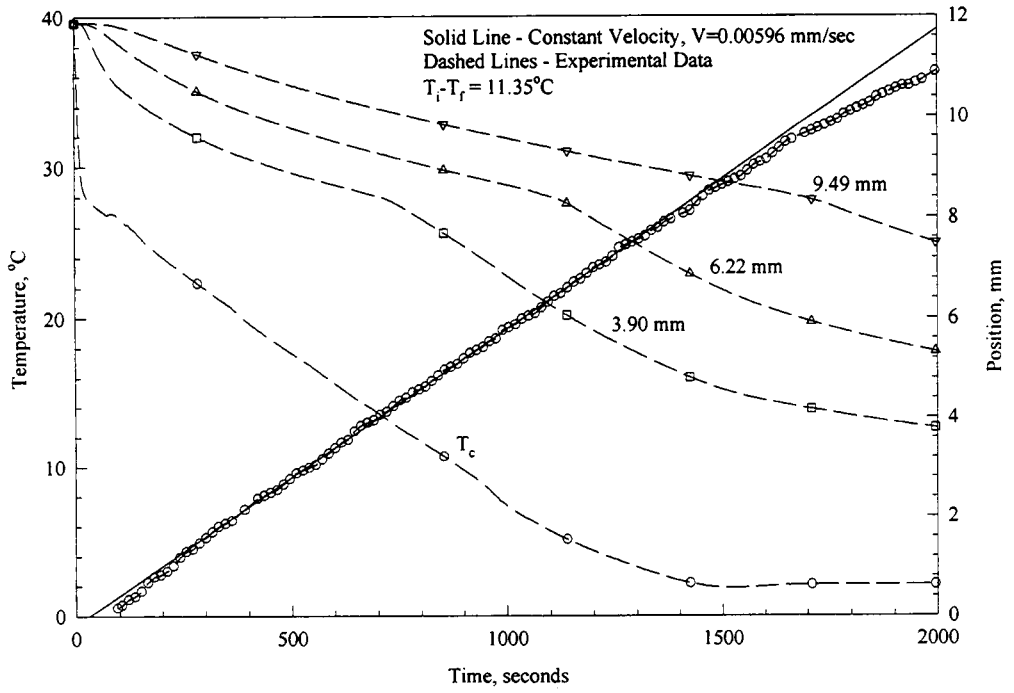


Figure 18: Run 7 Results

the measured front location was 0.028 mm with a maximum difference occurring at 660 seconds of 0.086 mm. This observation along with the results of the exact solution for the case of $T_i = T_f$ and V = constant suggest that the super heat of 11.35 °C, for n-octadecane is a minor factor in the solidification process if the boundary temperature is rapidly dropped to T_f.

Figure 19 shows a comparison of the front motions and the cold boundary temperatures for Runs 4 and 7. During the time span of nearly linear decrease in $T_c(t)$, constant front velocity solidification process is observed for both runs. As expected, Run 4 with negligible superheat resulted in a higher average front velocity than Run 7 where the superheat was 11.35 °C.

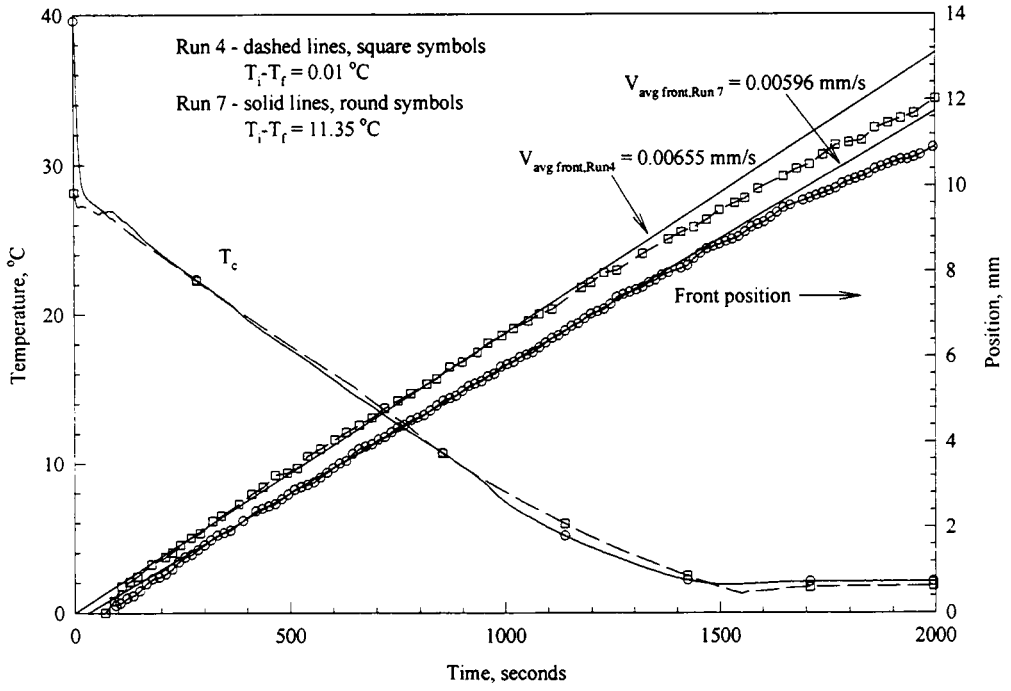


Figure 19:Comparison of Runs 4 and 7

Figure 20 shows the results from Run 8. The purpose of this run is to provide numerical researchers with accurate front movement data for a melt with an initial superheat subjected to a complicated boundary condition. The probes were measured to be 3.37, 5.95, and 9.23 mm respectively. These measurements are from the heat exchanger surface to the bottom of the probes. The effective locations of the probes were found to be 3.81, 6.56, and 9.56 mm, respectively. In this run, the boundary temperature was dropped rapidly to about T_f, then decreased linearly to about 6.6 °C and held at that value for about 227 seconds. Thereafter, it was linearly increased to about 10.6 °C and held at that value for about 980 seconds. Finally, the boundary temperature was again

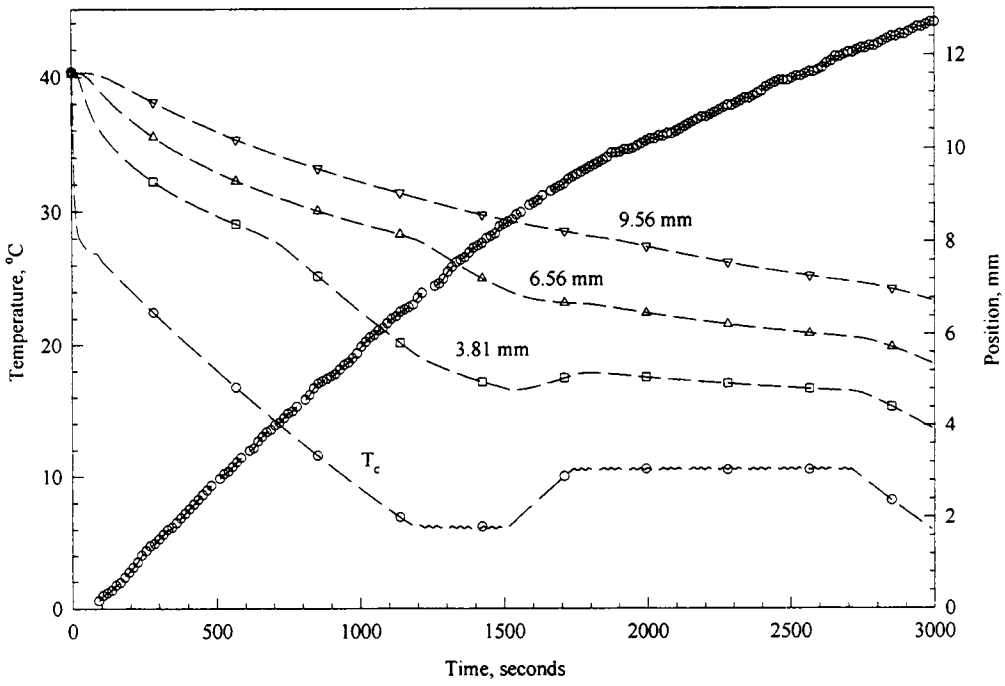


Figure 20: Run 8 Results, $T_i = 40.30$ °C

linearly decreased. These complicated changes in $T_c(t)$, especially the heating portion, provide a serious challenge to any inverse analysis method which is supposed to predict the $T_c(t)$ just based on the front data.

Figure 21 is a plot of the data from Run 9. The purpose was to perform a similar experiment to Run 8 but to lower the initial superheat of the material. The initial temperature of the melt was lowered to approximately 29.6 °C. An approximately 1.5 °C superheat was maintained to guard against the needling solidification on the sides of the test cell that complicated the front measurement in Run 5. The probes were measured to be 3.37, 5.95, and 9.23 mm respectively, and were taken from the heat exchanger surface to the bottom of the probes. The effective thermal locations of the probes were found to be 3.44, 6.00, and 9.68 mm.

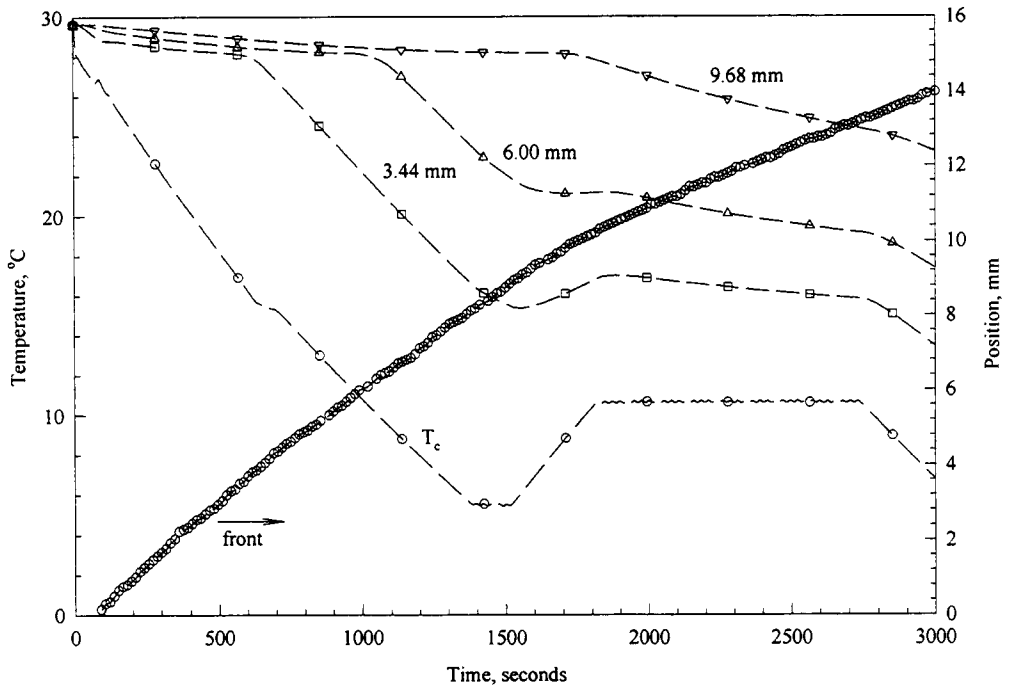


Figure 21: Run 9 Results, T_i = 29.60 °C

Chapter 4
Conclusions and Recommendations

The experimental setup and procedure presented here were successful in providing very accurate front location and boundary temperature information for the one-dimensional solidification of n-octadecane. For the initial runs, the data taken very closely reflected the exact solutions that were available with all discrepancies explained either by a physical phenomenon not considered in the exact solution (supercooling of the fluid at the heat exchanger surface) or by the inability of the setup to produce the specified boundary conditions assumed or calculated in the exact solutions(step change and linear heat exchanger temperature drops). The results show that for similar cooling conditions, the superheat of the melt proved to have a relatively small impact on the solidification rates. This is attributed to the material's high heat of fusion, and its relatively low specific heat as compared to the heat transfer rates during the experiments, i.e., the vast majority of the cooling went to solidifying the material rather than to cool the liquid from the superheat temperature down to the fusion temperature. The Stefan number represents the combination of these effects.

Two areas of improvement that could extend the capabilities of this setup are the front measurement technique and the temperature control of heat exchanger. The front location measurement for the current setup was limited by the amount of magnification possible with the camera while maintaining an acceptable focus on the ruler. The focus at higher magnifications was impaired by the light defraction as it passed through the curved

surfaces of the cylinder. Constructing a similar test cell using a Plexiglas cylinder with a flat side, either formed or machined into it, would alleviate the problems of defraction through the curved surface. This would allow the front measurement to be limited only by the capabilities of the video camera used. The heat exchanger temperature control could be improved by using alcohol as the cooling fluid rather than water. This would allow temperature ranges below 0 °C which would enable higher solidification rates to be studied.

The setup presented here, because of its ability to produce highly one-dimensional solidification, could also be used to study one-dimensional solidification of binary melts. However, the location of the mushy region-solid interface would present problems for the front measurement technique used here. This front measurement technique would be adequate to locate the liquid-mushy region interface if the mushy region were sufficiently opaque, but the mushy region-solid interface would have to be measured utilizing an alternate method.

Bibliography

Bibliography

[1] Ketkar, S. P., Parang, M., and Arimilli R. V., 'Experimental and Numerical Study of Solidification and Melting of Pure Materials,' *Journal of Thermophysics and Heat Transfer*, Vol. 5(1), 1989, pp. 40-45.

[2] Frankel, J. I. and Keyhani, M., 'A New Approach for Solving Inverse Solidification Design Problems', *Journal of Numerical Heat Transfer*, Part B, 1996, Vol. 30, No. 2, pp.161-177.

[3] Bathelt, A. J., Viskanta, R., and Leidenfrost, W., 'Latent Heat-of-Fusion Energy Storage: Experiments on Heat Transfer from Cylinders During Melting', *Journal of Heat Transfer*, Vol. 101, 1979, pp. 453-458.

[4] Bathelt, A. J. and Viskanta, R., 'Heat Transfer at the Solid-Liquid Interface During Melting from a Horizontal Cylinder', *International Journal of Heat and Mass Transfer*, Vol. 23, 1980, pp. 1493.

[5] Benard, G., Gobin, D., and Zanoli, A., 'Moving Boundary Problem: Heat Conduction in Solid Phase During Melting by Natural Convection in the Liquid', *International Journal of Heat and Mass Transfer*, Vol. 29(11), 1986,pp. 1669.

[6] Patankar, S. V. , 'Numerical Heat Transfer and Fluid Flow', Hemisphere, Washington, DC, 1980.

[7] Ho, C. J. and Viskanta, R., 'Inward Solid-Liquid Phase-Change Transfer in a Rectangular cavity with Conducting Vertical Walls', *International Journal of Heat and Mass Transfer*, Vol. 27(7), 1984, pp. 1055-1065.

[8] Moon-Hyun Chun, Heon-Oh Choi, Hyung-Gil Jun, and Yeon-Sik Kim, 'Phase-Change Front Prediction by Measuring the Wall Temperature on Which Solidification Occurs', *International Journal of Heat and Mass Transfer*, Vol. 30(12), 1987, pp. 2641-2650.

[9] McDonough, M. W. and Faghri, A., 'Ultrasonic Measurement of Solid-Liquid Interface for the Solidification of Water in a Rectangular Enclosure', *Journal of Heat Transfer*, Vol. 115, 1993, pp. 1075-1078.

[10]Parson, J. R., Irby, R. G., and Keshok, E. G., 'An Investigation of the Thermal Transport Properties of Octadecane', In *Proceedings of the 19th International Thermal Conduction Conference,* Tennessee Technological University, Cookeville, TN, October 1985.

[11]Jin, Y. and Wunderlich, B., 'Heat Capacities of Paraffins and Polyethylene', *Journal of Physical Chemistry*, Vol. 95, 1991.

[12]Carslaw, H. S. and Jaeger, J. C., 'Conduction of Heat in Solids', Clarendon Press, Oxford, 1959.

[13]Alexiades. V., 'Mathematical Modeling of Melting and Freezing Processes', Hemisphere Publishing Corporation, Washington, 1993.

[14]Poulikakos, D., 'Conduction Heat Transfer', Prentice Hall, Englewood Cliffs, New Jersey, 1994.

Appendix

Experimental Data

The following figures and tables present the data for all the runs discussed earlier. The front data is given in a tabular form in its entirety, while the cold boundary temperature, T_c, is given only in graphical form. Least squares polynomial curve fits have been included on the graphs for numerical purposes. The coefficients for the curve fits are given in the following tables. All curve fits are of the form

$$T_c = b_0 + b_1 t + b_2 t^2 + b_3 t^3 + b_4 t^4 + b_5 t^5$$

where T_c is the cold boundary temperature and t is the time in seconds.

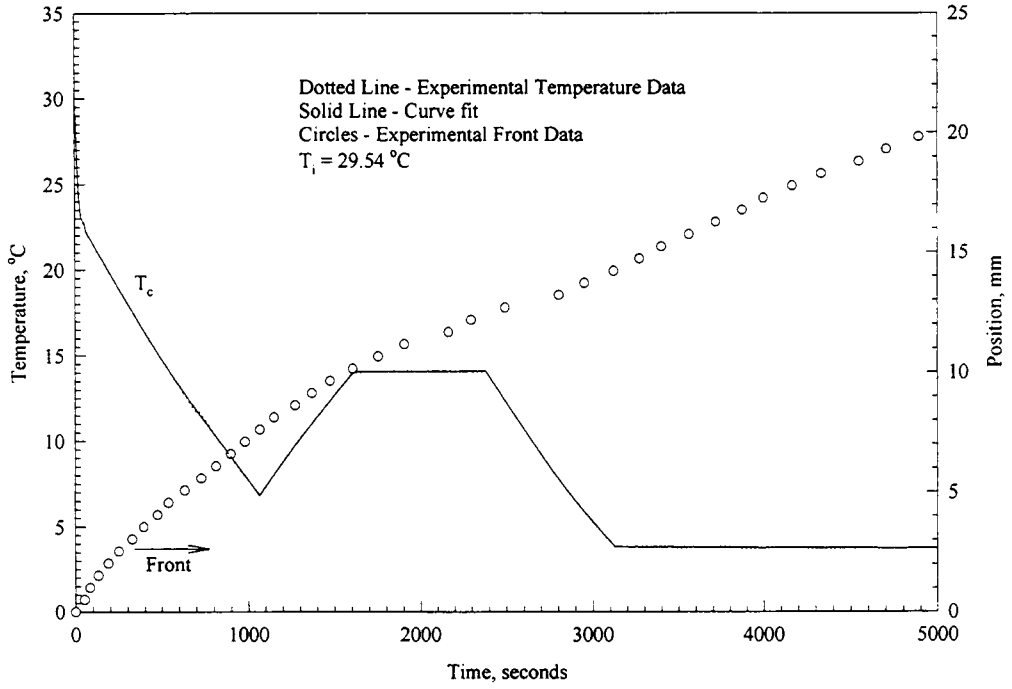


Figure 22: Run 1 Data

Table 7: Coefficients of boundary condition curve fit for Run 1

	Coefficients					
Time, seconds	b_0	b_1	b_2	b_3	b_4	b_5
$0 \le t \le 64.74$	2.9843235E+01	-1.7090934E-01	-1.3432010E-02	6.5550409E-04	-1.0099980E-05	5.2135083E-08
$64.74 \le t \le 1067.30$	2.3360735E+01	-1.7457795E-02	-4.4510848E-06	1.5418396E-08	-1.2215672E-11	3.0812297E-15
$1067.30 \le t \le 1613.10$	1.6343983E+02	-6.4770671E-01	1.0074934E-03	-7.5764622E-07	2.8192488E-10	-4.1646166E-14
$1613.10 \le t \le 2382.74$	1.4020198E+01	2.4735267E-05	0	0	0	0
$2382.74 \le t \le 3128.67$	1.4363714E+03	-2.6837370E+00	2.0485686E-03	-7.8302741E-07	1.4884887E-10	-1.1242850E-14
$3128.67 \le t \le 5000$	3.9816694E+00	-5.5691666E-05	0	0	0	0

Table 8: Front position data for Run 1

Time, seconds	Front position, mm
0	0.00
53	0.51
84	1.02
133	1.52
190	2.03
250	2.54
328	3.05
395	3.56
475	4.06
539	4.57
634	5.08
728	5.59
814	6.10
899	6.60
982	7.11
1070	7.62
1152	8.13
1274	8.64
1371	9.14
1475	9.65
1607	10.16
1754	10.67
1907	11.18
2165	11.68
2298	12.19
2494	12.70
2807	13.21
2954	13.72
3123	14.22
3273	14.73
3400	15.24
3563	15.75
3719	16.26
3876	16.76
4001	17.27
4168	17.78
4334	18.29
4551	18.80
4708	19.30
4892	19.81
5055	20.32

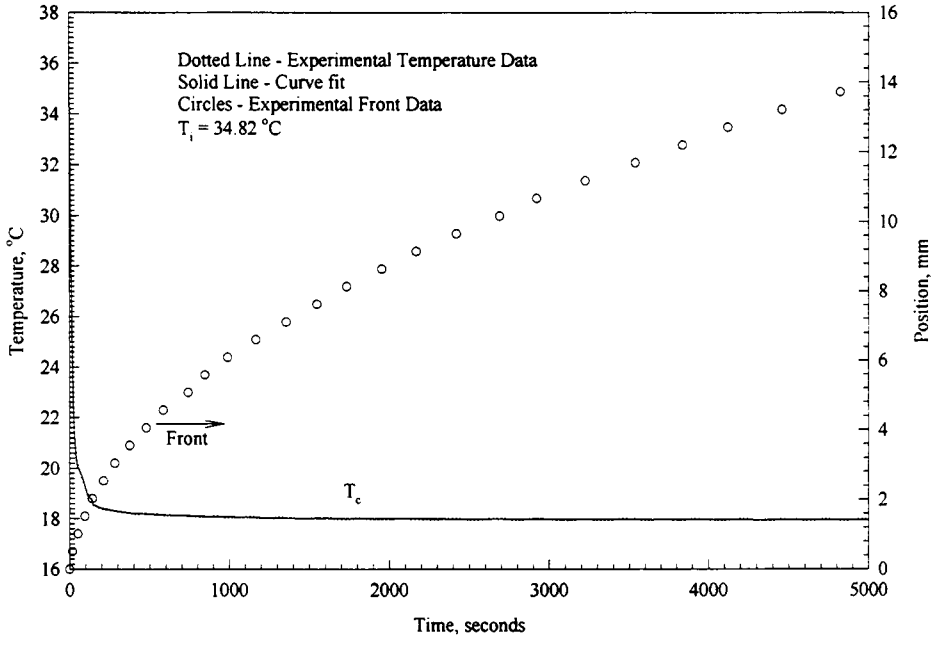


Figure 23: Run 2 data

Table 9 : Coefficients of boundary condition curve fit for Run 2

	Coefficients					
time, seconds	b_0	b_1	b_2	b_3	b_4	b_5
$0 \le t \le 64.74$	3.5792992E+01	-9.5067289E-01	2.2445441E-02	-2.5749152E-04	1.4124068E-06	-2.9732413E-09
$64.74 \le t \le 1067.30$	1.9150786E+01	-5.9289039E-03	1.4914586E-05	-1.9400841E-08	1.2460255E-11	-3.1319394E-15
$1067.30 \le t \le 1613.10$	1.8028072E+01	-1.8741269E-05	0	0	0	0

Table 10: Front position data for Run 2

Time, seconds	Front position, mm
0	0.00
18	0.51
52	1.02
96	1.52
143	2.03
212	2.54
282	3.05
375	3.56
479	4.06
586	4.57
744	5.08
850	5.59
993	6.10
1170	6.60
1358	7.11
1550	7.62
1735	8.13
1955	8.64
2170	9.14
2422	9.65
2693	10.16
2924	10.67
3227	11.18
3540	11.68
3840	12.19
4122	12.70
4459	13.21
4822	13.72
5164	14.22
3273	14.73
3400	15.24
3563	15.75
3719	16.26
3876	16.76
4001	17.27
4168	17.78
4334	18.29
4551	18.80
4708	19.30
4892	19.81
5055	20.32

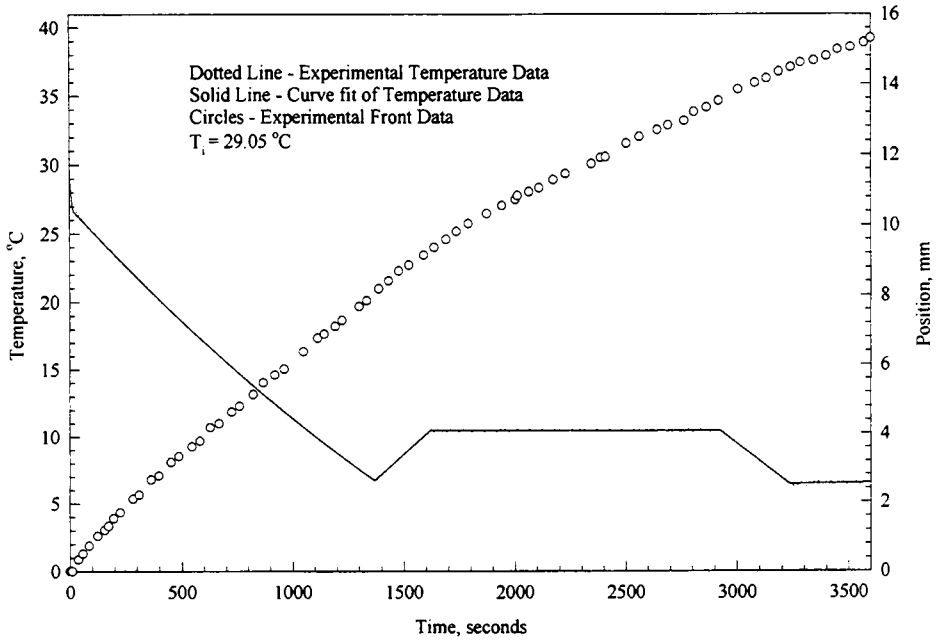


Figure 24: Run 3 Data

Table 11 : Coefficients of boundary condition curve fit for Run 3

	Coefficients					
Time, seconds	b_0	b_1	b_2	b_3	b_4	b_5
$0 \le t \le 16.57$	2.9039103E+01	-1.4320972E-01	0	0	0	0
$16.57 \le t \le 1369.08$	2.6958069E+01	-1.7683691E-02	2.1172631E-06	0	0	0
$1369.08 \le t \le 1619.48$	-1.3815586E+01	1.4996887E-02	0	0	0	0
$1619.48 \le t \le 2925.65$	1.0502209E+01	-1.8937398E-05	0	0	0	0
$2925.65 \le t \le 3236.09$	4.8392725E+01	-1.2970063E-02	0	0	0	0
$3236.09 \le t \le 3600.00$	5.3339404E+00	3.3572925E-04	0	0	0	0

Table 12: Front position data for Run 3

Time, seconds	Front position, mm
0	0
9	0
37	0.34
57	0.51
85	0.73
123	1.02
155	1.19
172	1.30
195	1.52
225	1.69
282	2.09
310	2.20
364	2.65
398	2.77
453	3.16
487	3.33
546	3.61
582	3.78
629	4.18
669	4.29
726	4.63
762	4.80
824	5.14
870	5.48
922	5.70
963	5.87
1050	6.38
1115	6.77
1144	6.89
1193	7.11
1224	7.28
1301	7.68
1335	7.85
1389	8.18
1433	8.41
1479	8.69
1525	8.86
1592	9.14
1639	9.37
1692	9.60
1739	9.82
1792	10.05
1875	10.33
1943	10.56
2003	10.72
2013	10.84
2066	10.95
2111	11.06
2175	11.29
2229	11.46
2346	11.74
2388	11.91
2410	11.94
2504	12.32
2563	12.51
2644	12.70
2693	12.83
2766	12.95
2809	13.21
2866	13.34
2920	13.53
3007	13.84
3082	14.03
3133	14.16
3187	14.35
3241	14.48
3285	14.61
3345	14.67
3401	14.80
3451	14.99
3509	15.05
3569	15.18
3599	15.30

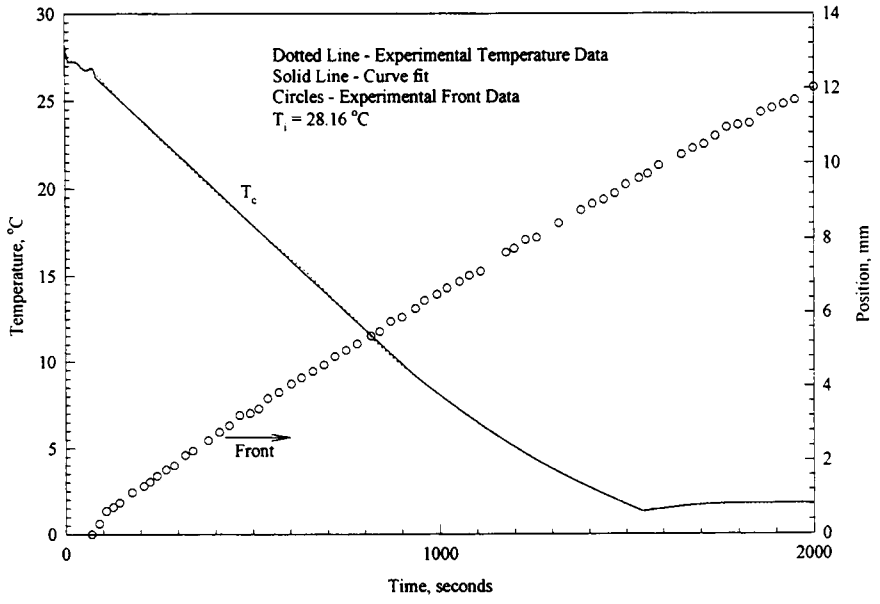


Figure 25: Run 4 data

Table 13: Coefficients of boundary condition curve fit for Run 4

	Coefficients					
time, seconds	b_0	b_1	b_2	b_3	b_4	b_5
$0 \le t \le 82.89$	2.8221121E+01	-1.8631651E-01	1.2618274E-02	-3.7735994E-04	4.9315448E-06	-2.3256563E-08
$82.89 \le t \le 936.21$	2.8036365E+01	-2.0191880E-02	0	0	0	0
$936.21 \le t \le 1542.35$	2.9273752E+01	-4.0178667E-02	5.6079747E-05	-6.8464811E-08	3.9723437E-11	-8.3631581E-15
$1542.35 \le t \le 2000.00$	4.9285774E+03	-1.3983730E+01	1.5813111E-02	-8.9090225E-06	2.5015005E-09	-2.8011309E-13

Table 14: Front position data for Run 4

Time, seconds	Front position, mm
70	0.00
90	0.28
108	0.62
127	0.73
144	0.85
177	1.13
209	1.30
225	1.41
244	1.58
268	1.75
290	1.86
319	2.14
339	2.26
380	2.54
410	2.77
437	2.94
465	3.22
493	3.27
516	3.39
540	3.67
570	3.84
603	4.06
630	4.23
660	4.40
690	4.57
720	4.80
750	4.97
780	5.14
817	5.36
840	5.48
870	5.76
900	5.87
936	6.10
960	6.32
993	6.49
1020	6.66
1054	6.83
1080	7.00
1110	7.11
1178	7.62
1200	7.73
1230	7.96
1260	8.02
1320	8.41
1380	8.75
1410	8.92
1440	9.03
1470	9.20
1500	9.43
1536	9.60
1560	9.71
1590	9.93
1650	10.22
1680	10.39
1710	10.50
1740	10.72
1770	10.95
1800	11.01
1830	11.06
1860	11.35
1890	11.46
1920	11.57
1950	11.68
2000	12.02

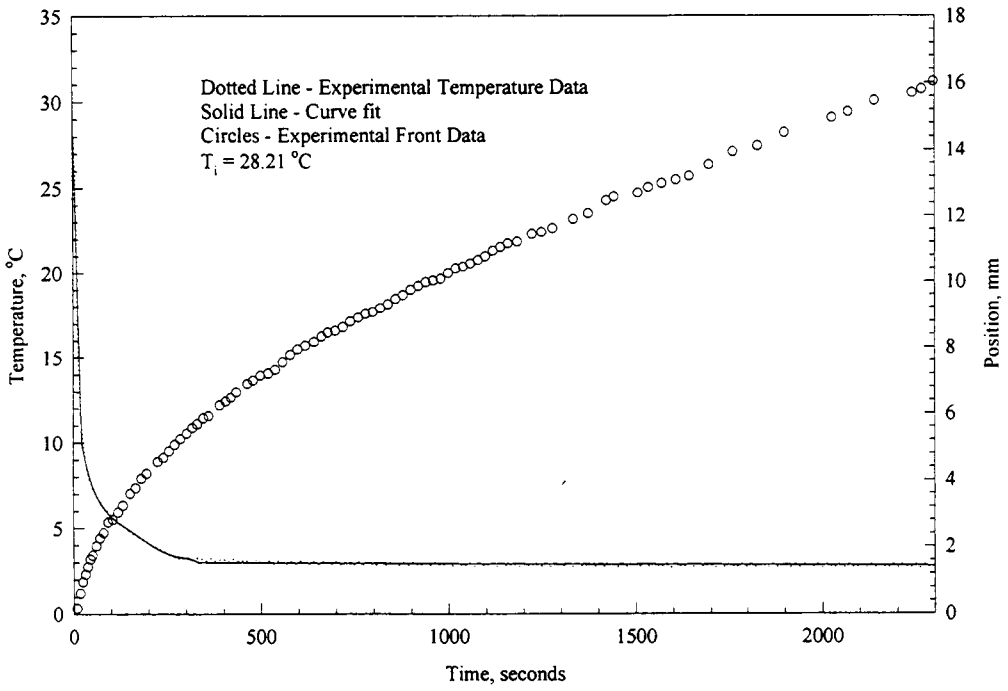


Figure 26: Run 5 data

Table 15: Coefficients of boundary condition curve fit for Run 5

	Coefficients					
time, seconds	b_0	b_1	b_2	b_3	b_4	b_5
$0 \le t \le 22.09$	2.9117048E+01	-8.6633813E-01	0	0	0	0
$22.09 \le t \le 332.22$	1.3351775E+01	-1.9040660E-01	1.9266928E-03	-1.0276176E-05	2.6394858E-08	-2.5819366E-11
$332.22 \le t \le 2300.00$	3.0219334E+00	-1.0585792E-04	0	0	0	0

Table 16 : Front position data for Run 5

Time, seconds	Front position, mm
9	0.17
18	0.62
25	0.96
32	1.18
38	1.41
45	1.64
51	1.75
61	2.03
70	2.26
80	2.43
92	2.74
105	2.82
119	3.05
132	3.25
151	3.61
166	3.78
181	4.06
195	4.22
225	4.57
240	4.68
255	4.88
270	5.08
285	5.25
302	5.42
317	5.59
330	5.70
346	5.87
360	5.94
390	6.26
406	6.38
420	6.49
435	6.66
465	6.91
480	7.01
500	7.16
521	7.22
540	7.34
560	7.56
580	7.79
600	7.96
620	8.07
643	8.18
663	8.35
680	8.47
700	8.52
720	8.64
740	8.80
761	8.92
780	9.03
800	9.09
820	9.20
840	9.31
860	9.48
880	9.60
900	9.76
920	9.88
940	9.99
960	10.05
980	10.10
1000	10.27
1020	10.41
1040	10.46
1060	10.56
1080	10.67
1100	10.78
1120	10.95
1140	11.06
1160	11.18
1185	11.23
1224	11.46
1250	11.52
1280	11.63
1335	11.91
1375	12.08
1423	12.48
1443	12.59
1507	12.70
1535	12.87
1571	12.98
1609	13.10
1644	13.21
1697	13.55
1762	13.94
1829	14.11
1901	14.51
2027	14.96
2070	15.13
2140	15.46
2240	15.69
2265	15.80
2296	16.03
2333	16.14
2400	16.26

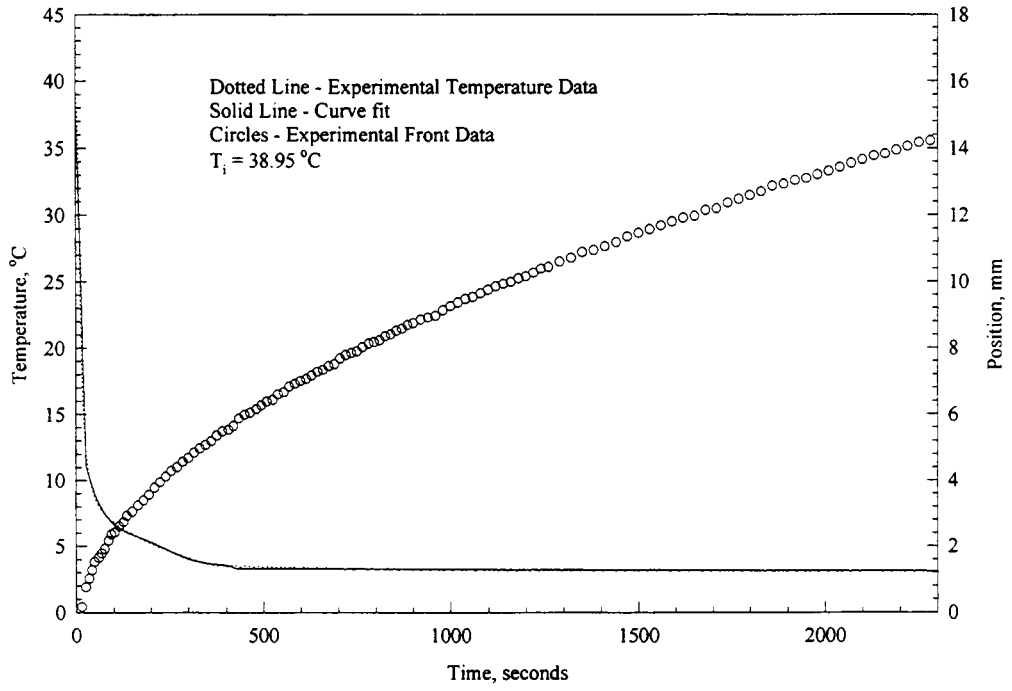


Figure 27 : Run 6 data

Table 17: Coefficients of boundary condition curve fit for Run 6

	Coefficients					
Time, seconds	b_0	b_1	b_2	b_3	b_4	b_5
$0 \le t \le 27.08$	3.8199837E+01	-9.9969821E-01	0	0	0	0
$27.08 \le t \le 426.03$	1.5180282E+01	-1.8735864E-01	1.5667596E-03	-6.6727144E-06	1.3504033E-08	-1.0354058E-11
$426.03 \le t \le 3000$	3.3519204E+00	-1.0705633E-04	0	0	0	0

Table 18: Front position data for Run 6

Time, seconds	Front position, mm
15	0.17
26	0.76
35	1.02
42	1.27
49	1.52
60	1.65
68	1.78
76	1.91
86	2.16
94	2.35
103	2.41
115	2.60
127	2.73
135	2.92
150	3.05
165	3.24
180	3.39
195	3.56
210	3.78
225	3.95
240	4.12
255	4.29
270	4.40
285	4.57
300	4.68
315	4.85
330	4.97
345	5.08
360	5.19
375	5.36
390	5.48
407	5.53
420	5.64
435	5.87
450	5.98
465	6.04
482	6.15
495	6.27
510	6.38
525	6.43
540	6.60
555	6.66
570	6.83
585	6.91
600	7.00
615	7.06
630	7.17
646	7.28
660	7.34
675	7.45
690	7.51
705	7.68
720	7.79
735	7.85
750	7.90
765	8.02
781	8.13
795	8.18
810	8.24
825	8.35
840	8.41
855	8.52
870	8.58
885	8.69
900	8.75
920	8.86
940	8.92
960	8.97
980	9.14
1000	9.26
1020	9.37
1040	9.48
1060	9.54
1080	9.65
1100	9.75
1120	9.86
1140	9.93
1160	9.99
1180	10.10
1200	10.16
1220	10.27
1240	10.39
1260	10.44
1290	10.61
1320	10.72
1350	10.89
1380	10.95
1410	11.06
1440	11.18
1470	11.35
1500	11.46
1530	11.57
1560	11.68
1590	11.80
1620	11.91
1650	11.97
1680	12.14
1710	12.19
1740	12.36
1770	12.47
1800	12.59
1830	12.70
1860	12.87
1890	12.93
1920	13.04
1950	13.10
1980	13.21
2010	13.32
2040	13.43
2070	13.55
2100	13.66
2130	13.77
2160	13.83
2190	13.94
2220	14.05
2250	14.17
2280	14.22
2310	14.34
2340	14.45
2373	14.62
2400	14.68
2430	14.73
2460	14.84
2491	14.96
2524	15.13
2550	15.18
2610	15.30
2651	15.41
2671	15.47
2700	15.52
2730	15.58
2760	15.69
2790	15.80
2820	15.92
2850	16.03
2880	16.14
2910	16.20
2940	16.26
2970	16.31
3000	16.48

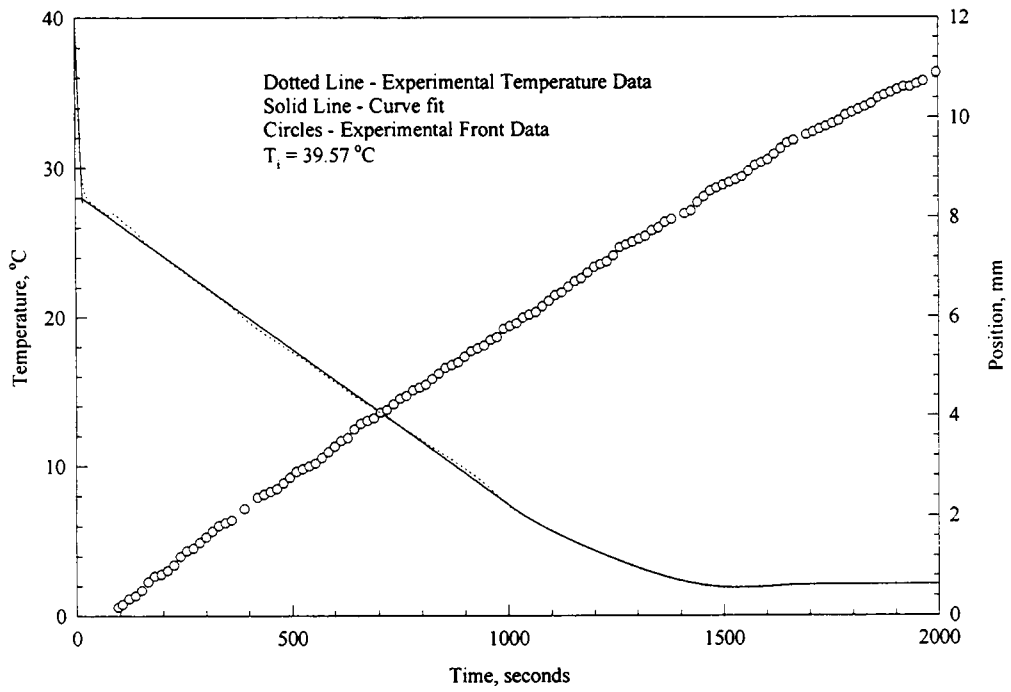


Figure 28 : Run 7 data

Table 19: Coefficients of boundary condition curve fit for Run 7

	Coefficients					
time, seconds	b_0	b_1	b_2	b_3	b_4	b_5
$0 \le t \le 15.56$	3.9744532E+01	-7.5484699E-01	0	0	0	0
$15.56 \le t \le 1022.50$	2.8322650E+01	-2.0883861E-02	0	0	0	0
$1022.50 \le t \le 1660.52$	6.9431399E+02	-2.5877388E+00	3.9242542E-03	-2.9798308E-06	1.1244474E-09	-1.6802722E-13
$1660.52 \le t \le 2000$	1.7792869E+00	1.6005827E-04	0	0	0	0

Table 20 : Front position data for Run 7

Time, seconds	Front position, mm
95	0.17
105	0.23
120	0.34
135	0.40
150	0.51
165	0.68
180	0.79
195	0.83
210	0.90
225	1.02
240	1.19
255	1.30
270	1.35
285	1.47
300	1.58
315	1.69
330	1.81
345	1.86
360	1.92
390	2.14
420	2.37
435	2.43
450	2.48
465	2.54
480	2.65
495	2.77
510	2.88
525	2.94
540	2.99
555	3.05
570	3.16
585	3.27
600	3.39
615	3.50
630	3.56
645	3.73
660	3.84
675	3.89
690	3.95
705	4.06
720	4.12
735	4.23
750	4.35
765	4.40
780	4.52
795	4.57
810	4.63
825	4.74
840	4.85
855	4.97
870	5.02
885	5.08
900	5.19
915	5.31
930	5.36
945	5.42
960	5.53
975	5.59
990	5.76
1005	5.81
1020	5.87
1035	5.98
1050	6.04
1065	6.10
1080	6.21
1095	6.32
1110	6.43
1125	6.49
1140	6.60
1155	6.72
1170	6.77
1185	6.89
1200	7.00
1215	7.06
1230	7.11
1245	7.22
1260	7.39
1275	7.45
1290	7.51
1305	7.56
1320	7.62
1335	7.73
1350	7.79
1365	7.90
1380	7.96
1410	8.07
1425	8.13
1440	8.30
1455	8.41
1470	8.52
1485	8.58
1500	8.64
1515	8.69
1530	8.75
1545	8.81
1560	8.92
1575	9.03
1590	9.09
1605	9.14
1620	9.26
1635	9.37
1650	9.48
1665	9.54
1695	9.65
1710	9.71
1725	9.76
1740	9.82
1755	9.88
1770	9.93
1785	10.05
1800	10.10
1815	10.16
1830	10.22
1845	10.27
1860	10.39
1875	10.44
1890	10.50
1905	10.56
1920	10.61
1935	10.61
1950	10.67
1965	10.72
1995	10.89
2010	10.95
2025	11.01
2040	11.06

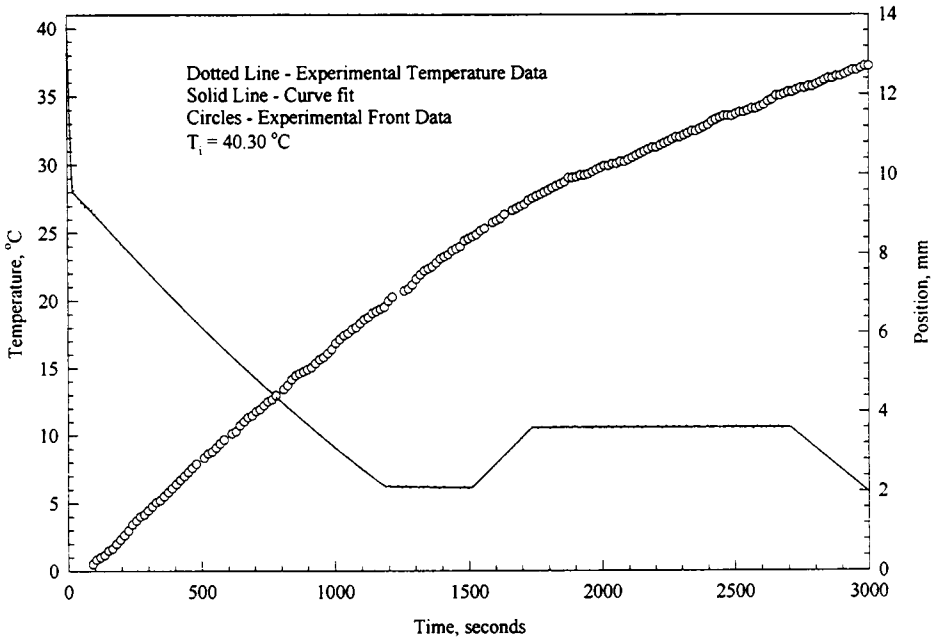


Figure 29: Run 8 data

Table 21: Coefficients of boundary condition curve fit for Run 8

	Coefficients					
Time, seconds	b_0	b_1	b_2	b_3	b_4	b_5
$0 \le t \le 18.26$	3.9878937E+01	-6.4691563E-01	0	0	0	0
$18.26 \le t \le 1187.36$	2.8434208E+01	-2.0158711E-02	-7.7657161E-06	2.0739002E-08	-1.7744785E-11	5.6068723E-15
$1187.36 \le t \le 1510.70$	6.6092486E+00	-3.1991498E-04	0	0	0	0
$1510.70 \le t \le 1737.82$	-2.3311566E+01	1.9486061E-02	0	0	0	0
$1737.82 \le t \le 2707.32$	1.0571144E+01	-1.1138429E-05	0	0	0	0
$2707.32 \le t \le 3000.00$	5.4647056E+01	-1.6291385E-02	0	0	0	0

Table 22: Front position data for Run 8

Time, seconds	Front position, mm
91	0.17
105	0.28
120	0.34
135	0.40
150	0.51
165	0.56
180	0.68
195	0.79
210	0.90
225	1.02
240	1.17
255	1.27
270	1.37
285	1.42
300	1.52
315	1.63
330	1.73
345	1.78
360	1.88
375	1.98
390	2.08
405	2.18
420	2.29
435	2.39
450	2.49
465	2.59
480	2.69
510	2.84
525	2.95
540	3.00
555	3.10
570	3.20
585	3.30
615	3.45
630	3.51
645	3.66
660	3.76
675	3.86
690	3.91
705	4.01
720	4.06
735	4.17
750	4.27
765	4.32
780	4.42
810	4.57
825	4.67
840	4.83
855	4.93
870	4.98
885	5.03
900	5.08
915	5.13
930	5.23
945	5.33
960	5.38
975	5.49
990	5.59
1005	5.74
1020	5.84
1035	5.94
1050	5.99
1065	6.10
1080	6.15
1095	6.25
1110	6.35
1125	6.40
1140	6.50
1155	6.55
1170	6.60
1185	6.65
1200	6.81
1215	6.91
1260	7.06
1275	7.11
1290	7.21
1305	7.37
1320	7.47
1335	7.57
1350	7.62
1365	7.67
1380	7.77
1395	7.87
1410	7.92
1425	7.98
1440	8.08
1455	8.13
1470	8.18
1485	8.33
1500	8.38
1515	8.43
1530	8.48
1545	8.59
1560	8.64
1590	8.79
1605	8.84
1620	8.89
1635	8.99
1665	9.09
1680	9.14
1695	9.19
1710	9.25
1725	9.35
1740	9.40
1755	9.45
1770	9.50
1785	9.55
1800	9.60
1815	9.65
1830	9.70
1845	9.75
1860	9.80
1875	9.91
1890	9.91
1905	9.93
1920	9.98
1935	9.98
1950	10.01
1965	10.06
1980	10.11
1995	10.16
2010	10.21
2025	10.21
2040	10.26
2055	10.26
2070	10.31
2085	10.31
2100	10.36
2115	10.41
2130	10.46
2145	10.52
2160	10.57
2175	10.62
2190	10.67
2205	10.67
2220	10.72
2235	10.77
2250	10.82
2265	10.87
2280	10.92
2295	10.92
2310	10.97
2325	11.02
2340	11.07
2355	11.07
2370	11.13
2385	11.18
2400	11.23
2415	11.31
2430	11.36
2445	11.41
2460	11.45
2475	11.45
2490	11.45
2505	11.50
2520	11.55
2535	11.55
2550	11.59
2565	11.64
2580	11.64
2595	11.68
2610	11.73
2625	11.82
2640	11.87
2655	11.96
2670	11.96
2685	12.01
2700	12.05
2715	12.05
2730	12.10
2745	12.15
2760	12.15
2775	12.19
2790	12.19
2805	12.24
2820	12.29
2835	12.34
2850	12.40
2865	12.40
2880	12.45
2895	12.45
2910	12.50
2925	12.55
2940	12.60
2955	12.60
2970	12.65
2985	12.70
3000	12.70

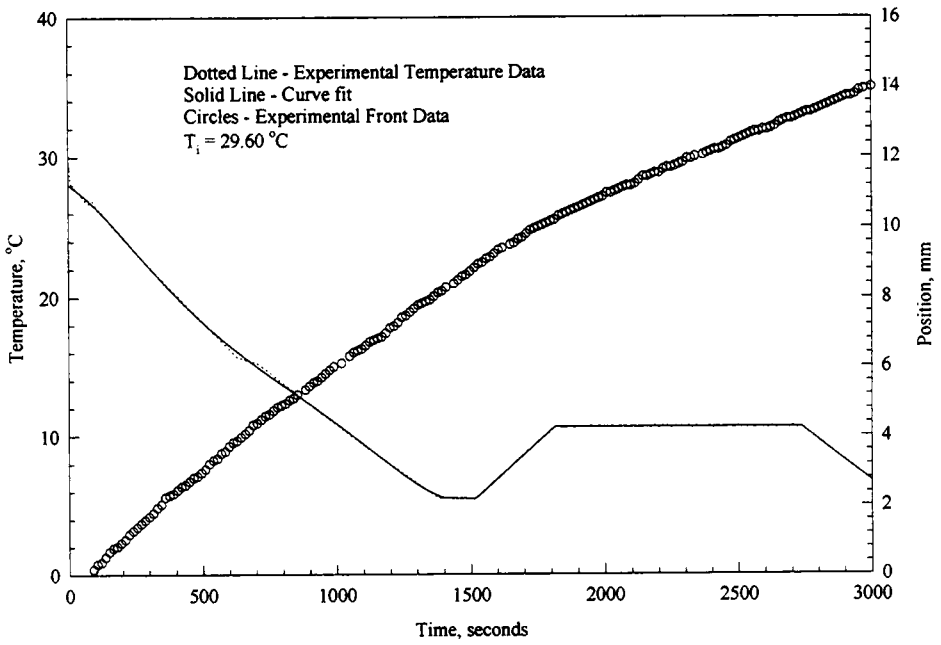


Figure 30: Run 9 data

Table 23: Coefficients of boundary condition curve fit for Run 9

	Coefficients					
Time, seconds	b_0	b_1	b_2	b_3	b_4	b_5
$0 \le t \le 11.86$	2.9723533E+01	-1.5443486E-01	0	0	0	0
$11.86 \le t \le 1399.35$	2.8039368E+01	-1.1884412E-02	-4.8189971E-05	9.8763589E-08	-7.6711270E-11	2.0873779E-14
$1399.35 \le t \le 1517.01$	6.1770452E+00	-4.6171269E-04	0	0	0	0
$1517.01 \le t \le 1814.89$	-2.0758345E+01	1.7293872E-02	0	0	0	0
$1814.89 \le t \le 2737.37$	1.0637488E+01	-5.1853456E-06	0	0	0	0
$2737.37 \le t \le 3000.00$	5.1159264E+01	-1.4808349E-02	0	0	0	0

Table 24: Front position data for Run 9

Time, seconds	Front position, mm
90	0.15
105	0.30
120	0.36
135	0.51
150	0.66
165	0.76
180	0.81
195	0.91
210	1.02
225	1.17
240	1.27
255	1.37
270	1.47
285	1.57
300	1.68
315	1.78
330	1.93
345	2.03
360	2.24
375	2.29
390	2.34
405	2.44
420	2.54
435	2.59
450	2.69
465	2.79
480	2.84
495	2.95
510	3.05
525	3.20
540	3.30
555	3.35
570	3.51
585	3.56
600	3.71
615	3.81
630	3.86
645	3.96
660	4.06
675	4.17
690	4.32
705	4.37
720	4.47
735	4.57
750	4.62
765	4.72
780	4.83
795	4.88
810	4.93
825	5.03
840	5.08
855	5.18
885	5.33
900	5.44
915	5.54
930	5.59
945	5.69
960	5.79
975	5.89
990	5.99
1020	6.10
1050	6.30
1065	6.40
1080	6.45
1095	6.50
1110	6.60
1125	6.71
1140	6.76
1155	6.81
1170	6.86
1185	6.96
1200	7.11
1215	7.16
1230	7.26
1245	7.42
1260	7.47
1275	7.57
1290	7.67
1305	7.77
1320	7.82
1335	7.87
1350	7.92
1365	8.03
1380	8.13
1395	8.18
1410	8.28
1440	8.38
1455	8.48
1470	8.59
1485	8.64
1500	8.74
1515	8.84
1530	8.94
1545	8.99
1560	9.09
1575	9.14
1590	9.25
1605	9.35
1620	9.40
1650	9.50
1665	9.55
1680	9.65
1695	9.70
1710	9.80
1725	9.91
1740	9.96
1755	10.01
1770	10.06
1785	10.11
1800	10.16
1815	10.21
1830	10.31
1845	10.36
1860	10.41
1875	10.46
1890	10.52
1905	10.57
1920	10.62
1935	10.67
1950	10.72
1965	10.77
1980	10.82
1995	10.87
2010	10.97
2025	10.97
2040	11.02
2055	11.07
2070	11.13
2085	11.18
2100	11.18
2115	11.23
2130	11.33
2145	11.43
2160	11.43
2175	11.48
2190	11.53
2205	11.53
2220	11.63
2235	11.68
2250	11.68
2265	11.73
2280	11.79
2295	11.84
2310	11.94
2325	11.94
2340	11.99
2370	12.04
2385	12.09
2400	12.14
2415	12.19
2430	12.19
2445	12.24
2460	12.29
2475	12.40
2490	12.45
2505	12.50
2520	12.55
2535	12.60
2550	12.65
2565	12.70
2580	12.70
2595	12.75
2610	12.75
2625	12.80
2640	12.85
2655	12.95
2670	13.00
2685	13.06
2700	13.06
2715	13.11
2730	13.16
2745	13.21
2760	13.26
2775	13.26
2790	13.31
2805	13.36
2820	13.41
2835	13.46
2850	13.51
2865	13.56
2880	13.61
2895	13.67
2910	13.72
2925	13.72
2940	13.77
2955	13.87
2972	13.92
3000	13.97

Vita

Shawn Wesley was born in Oak Ridge, Tennessee on September 14, 1971. He graduated from Oak Ridge High School in June of 1989 and attended Roane State Community College for one year. He entered the Tennessee Technological University in Cookeville, Tennessee in the fall semester of 1990. He received a Bachelor of Science Degree in Mechanical Engineering in the summer of 1994 and entered into the University of Tennessee mechanical engineering program and received his Master of Science Degree in the fall of 1996.